Energy-controlling time integration methods for nonlinear elastodynamics and low-velocity impact

Patrice Hauret, Patrick Le Tallec

Energy-controlling time integration methods for nonlinear elastodynamics and low-velocity impact

Patrice Hauret [a] and Patrick Le Tallec [b,*]

[a] *Graduate Aeronautical Laboratories, MS 205-45, California Institute of Technology Pasadena, CA 91125, USA*

[b] *Laboratoire de Mécanique des Solides, CNRS UMR 7649, Département de Mécanique, Ecole Polytechnique, 91128 Palaiseau Cedex, FRANCE*

Abstract

It is now well established that discrete energy conservation/dissipation plays a key-role for the unconditional stability of time integration schemes in nonlinear elastodynamics. In this paper, from a rigorous conservation analysis of the Hilber-Hughes-Taylor time integration scheme [1], we propose an original way of introducing a controllable energy dissipation while conserving momenta in conservative strategies like [2–5]. Moreover, we extend the technique proposed in [3] to provide energy-controlling time integration schemes for frictionless contact problems enforcing the standard Kuhn-Tucker conditions at time discretization points. We also extend this technique to viscoelastic models. Numerical tests involving the impact of incompressible elastic or viscoelastic bodies in large deformation are proposed to confirm the theoretical analysis.

Key words: Time integration schemes, Nonlinear elastodynamics, Energy-momenta conserving algorithms, Energy dissipation, Contact, Viscoelasticity
PACS: 02.60.Jh, 46.20, 46.30.J

* Corresponding author.
Email addresses: phauret@aero.caltech.edu (Patrice Hauret), patrick.letallec@polytechnique.fr (Patrick Le Tallec).

1 Introduction

Nonlinear structures were central in J. Argyris contributions, and in dedication to his work, the present paper discusses the time integration of such problems.

Time integration schemes for elastodynamics have been developed for a long time in a linear framework in which consistency and linear stability ensure convergence by time step refinement. Whereas the conditionally stable explicit centered method must be mentioned for its simplicity, the numerical stiffness of real mechanical problems has lead to the development of implicit methods, such as Houbolt, Wilson, Newmark or Hilber-Hughes-Taylor [1], especially when dealing with incompressible materials. These methods have been studied and used with great success in conjunction with finite element techniques to solve large scale industrial problems (see [6–8] among others). Nevertheless, when considering nonlinear problems, the previous implicit schemes lose their unconditional stability and many contributions along the years have proposed direct or indirect methods to overcome this difficulty.

In the Hamiltonian framework (i.e. when using conservative loadings), a geometrical approach could consist in constructing numerical schemes whose flow is symplectic [9,10], entailing the conservation of the volume in the phase space. Nevertheless, such a condition is not always sufficient to ensure the stability of the numerical system for large time steps and stiff problems, as observed by J.C.Simo and O.Gonzalez in [11] and illustrated numerically in this paper. Moreover, as mentioned by the authors, symplectic schemes seem difficult to build for nonlinearly kinematically constrained systems.

More recently, a variational understanding of time integration schemes in the Lagrangian framework has lead to the concept of variational integrators, and is detailed in [12,13]. An explicit asynchronous variant has also been proposed in [14]. The main interest of this approach is to provide an elegant and natural framework for the analysis of the geometrical properties of -in general- already existing strategies. Besides, a first convergence result has been recently obtained in the framework of Γ-convergence [15]. Still, the debate between geometric and purely conservative approaches remains very active.

The present paper opts for paying a direct attention to the local evolution of energy. A natural approach in this framework can consist in imposing energy conservation as a constraint, by projection [16,17] or by Lie group methods [18] but these methods are computationally expensive. By a mean value argument, Simo and Tarnow have shown in [2] that conservation could be achieved in a simpler way by solving a local nonlinear equation for the algorithmic second Piola-Kirchhoff stress tensor, which has lead to an implementation developed by Laursen and Meng in [4]. The variant proposed by Gonzalez in [3], reviewed

and developed herein replaces this nonlinear equation by an explicit formula which is simpler to implement. A recent alternative to this formulation consists in the time averaging of the stresses, as proposed by [5]. This approach of local averaging originates from time finite elements [19].

In addition, *linearly dissipative* integration schemes, i.e. schemes whose spectral radius is strictly less than unity, have been developed to avoid polynomial instabilities, such as those observed for non-diagonalizable integrators with multiple unit eigenvalue. But their use in nonlinear elastodynamics [20,21] can lead to poor conservation of momenta. Energy-dissipating momenta-conserving time integration schemes were then proposed in the nonlinear framework, in order to damp out unresolved high frequency modes while maintaining good accuracy (see Borri, Bottasso and Trainelli [22–24], Armero and Romero [20,21] or Bui [25] and the references therein), using modified integrations of the inertial term, or numerical Rayleigh dampings at high frequency [8]. In section 4, based on a rigorous analysis of the HHT scheme, we introduce energy dissipation in nonlinear conservative schemes by using non-trapezoidal second order approximation of the inertial term. The proposed modification only acts on the inertial terms, and therefore can be easily applied to all systems in which the potential energy is integrated by a conservative method.

Another important and difficult aspect of the dynamics of hyperelastic structures concerns low-velocity impact problems. Over the last years, an increasing interest has been devoted to energy-conserving time integration schemes for contact mechanics. In particular, in the framework of frictionless contact, both Laursen and Chawla [26] and Armero and Petöcz [27] have proposed energy-momenta conserving approaches. The key-point consists in an adequate discretization of the contact persistency condition, which must be compatible with the time integration strategy in order to achieve energy conservation. Nevertheless, as underlined in [28], both contributions encounter a difficulty in enforcing the unilateral conditions associated to frictionless contact, resulting into a small violation of the kinematical contact condition in order to conserve the main invariants in the dynamics. This drawback is overcome by Laursen and Love in [28], by introducing a discrete jump in velocities during impact. The enforcement of contact conditions at each time step is then possible at the computational price of resolving a problem on the jump in velocities. Such an additional computation is no more necessary in the approach proposed here in section 5. Indeed, when enforcing the contact condition by a penalty technique, by applying the correction technique of [3] to all penalty and energy terms involved in the mechanical problem, we propose in section 5 an energy-conserving scheme naturally enforcing the standard Kuhn-Tucker contact conditions at entire time steps.

Last, we show that energy correction techniques can also be extended to viscoelastic models, in order to ensure that the numerical scheme exactly respects

the physical energy dissipation.

The present paper is finally organized as follows. After a brief introduction of the equations of quasi-incompressible nonlinear elastodynamics (section 2), we propose (section 3) an energy conservation analysis of some standard time integration implicit strategies such as midpoint and trapezoidal rules. In particular, their major sources of instability are identified in presence of an incompressibility constraint, and their theoretical performances are then compared with the improved strategies of [2–4]. In section 4, based on a rigorous conservation analysis of the Hilber-Hughes-Taylor [1] time integration scheme, we propose an energy-controlling momenta-conserving time integration scheme using a simple modification of [3]. In particular, it is second order accurate and achieves an energy-decaying property for a regularized energy involving acceleration effects. In section 5, extensions of the energy correction technique from [3] are introduced to handle contact or viscoelastic problems. Two situations are considered: on one hand, we propose a time-integration strategy for penalized contact problems enabling the enforcement of the standard Kuhn-Tucker conditions at time discretization points. On the other hand, a time integration strategy with exact discrete balance is proposed for a viscoelastic model taken from [29]. The developed methods are tested in section 6 for the simulation of dynamic and impact problems involving compressible, incompressible elastic or viscoelastic bodies in large deformation.

2 Quasi-incompressible elastodynamics

2.1 The incompressible model

The open set $\Omega \subset \mathbb{R}^3$ denotes the interior of the reference configuration of a solid body and the map

$$\varphi : [0,T] \times \Omega \to \mathbb{R}^3$$

describes its time dependent deformation. The material is assumed to be incompressible in the sense that on $[0,T] \times \Omega$,

$$\det F = 1, \quad \text{with } F = \nabla \varphi.$$

The mass density of the material in the reference configuration is denoted by ρ and the body forces by $f : [0,T] \times \Omega \to \mathbb{R}^3$. The displacement $\varphi_D : [0,T] \times \Gamma_D \to \mathbb{R}^3$ and the traction $g : [0,T] \times \Gamma_N \to \mathbb{R}^3$ are prescibed respectively on the subsets Γ_D and Γ_N of the boundary $\Gamma = \partial\Omega$ of the domain, with $\overline{\Gamma_D \cup \Gamma_N} = \Gamma$, $\Gamma_D \cap \Gamma_N = \emptyset$. A contact surface will be considered as a traction boundary with unknown surface traction g and known constraints on the deformation φ.

The first and second Piola-Kirchhoff stress tensors in the material are denoted by Π and Σ, and given by the hyperelastic constitutive law:

$$\begin{aligned}\Sigma &= 2\frac{\partial \mathcal{W}}{\partial C} - 2p\frac{\partial \det C^{1/2}}{\partial C},\\ \Pi &= F\cdot\Sigma = \frac{\partial \hat{\mathcal{W}}}{\partial F} - p\, cof\, F\end{aligned} \tag{1}$$

Above, $p : [0,T]\times\Omega \to \mathbb{R}$ denotes the hydrostatic pressure, $\hat{\mathcal{W}}$ and $\mathcal{W}$ the stored elastic potentials respectively written in terms of the gradient F or the right Cauchy-Green strain tensor $C = F^t\cdot F$. The cofactor matrix of the matrix F is denoted by $cof\, F = \partial_F \det F$.

2.2 Variational quasi-incompressible formulation

Let us introduce variational spaces for displacements, velocities and pressures such as:

$$\begin{cases}\mathcal{U}_0 = \{u \in W^{1,s}(\Omega)^3; \quad u = 0 \text{ on } \Gamma_D\},\\ \mathcal{V} = \{w \in L^2(\Omega)^3\},\\ \mathcal{P} = \{p \in L^q(\Omega); \quad \frac{3}{s} + \frac{1}{q} \le 1\}.\end{cases} \tag{2}$$

Then, the variational formulation of the hyperelastic incompressible elastodynamics problem under consideration consists in finding

$$\begin{cases}\varphi - \varphi_D \in L^2(0,T;\mathcal{U}_0),\\ \dot{\varphi} \in L^2(0,T;\mathcal{V}),\\ p \in L^2(0,T;\mathcal{P}),\end{cases} \tag{3}$$

such that for any $v \in \mathcal{U}_0$, $w \in \mathcal{V}$ and $q \in \mathcal{P}$, the following equations hold in the sense of distributions:

$$\begin{cases}\partial_t \int_\Omega \rho\dot{\varphi}\cdot v + \int_\Omega \Pi : \nabla v = \int_\Omega f\cdot v + \int_{\Gamma_N} g\cdot v, \quad \text{in } \mathcal{D}'(0,T),\\ \partial_t \int_\Omega \varphi\cdot w = \int_\Omega \dot{\varphi}\cdot w, \quad \text{in } \mathcal{D}'(0,T),\\ \int_\Omega (\det\nabla\varphi - 1 + \epsilon p)\, q = 0, \quad \text{in } \mathcal{D}'(0,T).\end{cases} \tag{4}$$

Remark 1 *The spaces $\mathcal{U}_0$, $\mathcal{V}$ and $\mathcal{P}$ are replaced by finite dimensional spaces when using finite element approximations. The coefficient ϵ is zero for an incompressible material. It is positive and small for a compressible material with large bulk modulus $1/\epsilon$. For such materials, the weak formulation (4) leads to locking free finite element techniques.*

We have [30]:

Proposition 1 *The following conservation properties formally hold for a solution of (3) at any time $t \in [0, T]$:*

- *Energy conservation.*

$$\mathcal{E}(t) - \mathcal{E}(0) = \int_0^t \left(\int_\Omega f \cdot \dot{\varphi} + \int_{\Gamma_N} g \cdot \dot{\varphi} \right), \tag{5}$$

the total energy being defined by:

$$\mathcal{E}(t) = \frac{1}{2} \int_\Omega \rho \dot{\varphi}(t,x)^2 \, dx + \int_\Omega \hat{\mathcal{W}}(x, \nabla\varphi(t,x)) \, dx + \frac{\epsilon}{2} \int_\Omega p(t)^2. \tag{6}$$

- *Angular momentum conservation (for $\Gamma_D = \emptyset$).*

$$\mathcal{J}(t) - \mathcal{J}(0) = \int_0^t \left(\int_\Omega \varphi \times f + \int_{\Gamma_N} \varphi \times g \right), \tag{7}$$

with:

$$\mathcal{J}(t) = \int_\Omega \rho\varphi(t,x) \times \dot{\varphi}(t,x) \, dx. \tag{8}$$

- *Linear momentum conservation (for $\Gamma_D = \emptyset$).*

$$\mathcal{I}(t) - \mathcal{I}(0) = \int_0^t \left(\int_\Omega f + \int_{\Gamma_N} g \right), \tag{9}$$

with:

$$\mathcal{I}(t) = \int_\Omega \rho\dot{\varphi}(t,x) \, dx. \tag{10}$$

In the next sections, we are interested in the transposition of these conservation properties to the time discrete framework.

3 Conservation analysis for some usual schemes

In nonlinear elastodynamics, discrete energy dissipation at large (i.e. strict dissipation or conservation) is the natural criterion of stability for time integration schemes. Newmark's trapezoidal scheme, also known as the trapezoidal rule (see [6]), is the typical example of a scheme conserving mechanical energy. It is rather natural to study herein its possible generalizations to the nonlinear framework. The resulting analysis is well known but explains the difficulties encountered in nonlinear dynamics and leads to the design of improved nonlinear energy conserving schemes, as proposed in [2–4].

3.1 General time discrete formulation

The time interval $[0,T]$ is splitted into subintervals $[0,T] = \cup_{n=0}^{N}[t_n; t_{n+1}]$, with $\Delta t_n = t_{n+1} - t_n$, and we look at the family of second order accurate midpoint time integration schemes, of the form:

$$\begin{cases} \displaystyle\int_\Omega \rho\dot{\varphi}_{n+1}\cdot v = \int_\Omega \rho\dot{\varphi}_n\cdot v - \Delta t_n\int_\Omega \Pi_{n+1/2} : \nabla v \\ \qquad\qquad\qquad + \Delta t_n\displaystyle\int_\Omega \frac{f_n+f_{n+1}}{2}\cdot v + \Delta t_n\int_{\Gamma_N}\frac{g_n+g_{n+1}}{2}\cdot v, \\ \displaystyle\int_\Omega \varphi_{n+1}\cdot w = \int_\Omega \varphi_n\cdot w + \Delta t_n\int_\Omega \frac{\dot{\varphi}_n+\dot{\varphi}_{n+1}}{2}\cdot w, \\ \displaystyle\int_\Omega q\left(D_{n+1/2} - 1 + \epsilon\,\frac{p_n+p_{n+1}}{2}\right) = 0, \end{cases} \tag{11}$$

for any $v\in\mathcal{U}_0$, $w\in\mathcal{V}$, $q\in\mathcal{P}$, where $\square_n$ represents a discrete approximation of the quantity $\square(t_n)$ at time t_n. Any specific scheme of that family is entirely determined by the expressions of the first algorithmic Piola-Kirchhoff stress tensor $\Pi_{n+1/2}$ and the jacobian $D_{n+1/2}$. To achieve second order accuracy, one must satisfy:

$$\begin{cases} \Delta t_n\displaystyle\int_\Omega \Pi_{n+1/2} : \nabla v = \int_{t_n}^{t_{n+1}}\int_\Omega \Pi : \nabla v + O(\Delta t_n^3), \quad \forall v\in\mathcal{U}_0, \\ \Delta t_n\displaystyle\int_\Omega q\; D_{n+1/2} = \int_{t_n}^{t_{n+1}}\int_\Omega q\;\det C^{1/2} + O(\Delta t_n^3), \quad \forall q\in\mathcal{P}. \end{cases} \tag{12}$$

In the sequel, we will assume that the space $\mathcal{V}$ of velocities coincide with the space $\mathcal{U}_0$ of displacements. In this framework, velocities have a trace on Γ_N and the work of surfacic loadings has a proper meaning.

3.2 Trapezoidal rule

When approximating the time integrals in (12) by the trapezoidal rule, the so-called trapezoidal second order scheme is obtained, corresponding to the choice:

$$\begin{cases} \Pi_{n+1/2} := \dfrac{1}{2}\left(\dfrac{\partial\hat{\mathcal{W}}}{\partial F}(F_n) + \dfrac{\partial\hat{\mathcal{W}}}{\partial F}(F_{n+1})\right) - \dfrac{1}{2}\left(p_n\, cof\, F_n + p_{n+1}\, cof\, F_{n+1}\right), \\ D_{n+1/2} := \dfrac{1}{2}\left(\det F_n + \det F_{n+1}\right). \end{cases} \tag{13}$$

In other words, it is a stress averaging scheme, with

Proposition 2 *The trapezoidal rule achieves the following conservation properties:*

(1) Discrete energy.

$$\mathcal{E}_{n+1} - \mathcal{E}_n = \mathfrak{P}_n + c_n \Delta t_n^3, \tag{14}$$

where the discrete work between times t_n and t_{n+1} is given by:

$$\mathfrak{P}_n = \int_\Omega \frac{f_n + f_{n+1}}{2} \cdot (\varphi_{n+1} - \varphi_n) + \int_{\Gamma_N} \frac{g_n + g_{n+1}}{2} \cdot (\varphi_{n+1} - \varphi_n).$$

The scalar c_n only depends on φ_n, $\dot{\varphi}_n$, p_n, φ_{n+1}, $\dot{\varphi}_{n+1}$, p_{n+1}, and on the approximate time derivative of the pressure $\frac{p_{n+1}-p_n}{\Delta t_n}$. We will say that c_n only depends on the approximate solution at times n and $n+1$.

(2) Discrete angular momentum. *If $\Gamma_D = \emptyset$,*

$$\mathcal{J}_{n+1} - \mathcal{J}_n = \mathfrak{M}_n + c_n \Delta t_n^3, \tag{15}$$

where the resultant moment between times t_n and t_{n+1} is given by:

$$\mathfrak{M}_n = \Delta t_n \left(\int_\Omega \frac{\varphi_n + \varphi_{n+1}}{2} \times \frac{f_n + f_{n+1}}{2} + \int_{\Gamma_N} \frac{\varphi_n + \varphi_{n+1}}{2} \times \frac{g_n + g_{n+1}}{2} \right).$$

The constant c_n only depends on the approximate solution at times n and $n+1$.

(3) Discrete linear momentum. *If $\Gamma_D = \emptyset$,*

$$\mathcal{I}_{n+1} - \mathcal{I}_n = \mathfrak{F}_n, \tag{16}$$

where the resultant force between times t_n and t_{n+1} is given by:

$$\mathfrak{F}_n = \Delta t_n \left(\int_\Omega \frac{f_n + f_{n+1}}{2} + \int_\Gamma \frac{g_n + g_{n+1}}{2} \right).$$

Proof : The proof is quite classical and we refer to [31] for more details. We nevertheless briefly outline the calculation of energy and angular momentum evolutions to explain the numerical origin of energy conservation errors.

(1) Energy evolution. We take $v = (\varphi_{n+1} - \varphi_n)/\Delta t$ in (11). The inertial term gives the discrete increase of kinetic energy:

$$\int_\Omega \rho \left(\dot{\varphi}_{n+1} - \dot{\varphi}_n \right) \cdot v = \frac{1}{2} \int_\Omega \rho \dot{\varphi}_{n+1}^2 - \frac{1}{2} \int_\Omega \rho \dot{\varphi}_n^2.$$

The elastic term gives by a standard Taylor's expansion:

$$\begin{aligned}
&\frac{1}{2}\left(\frac{\partial\hat{\mathcal{W}}}{\partial F}(F_n)+\frac{\partial\hat{\mathcal{W}}}{\partial F}(F_{n+1})\right):(F_{n+1}-F_n)\,,\\
&=\left(\hat{\mathcal{W}}_{n+1}-\hat{\mathcal{W}}_n\right)+c\frac{\partial^3\mathcal{W}}{\partial F^3}(F_*)(F_{n+1}-F_n)^3,\\
&=\left(\hat{\mathcal{W}}_{n+1}-\hat{\mathcal{W}}_n\right)+\frac{c}{8}\Delta t_n^3\frac{\partial^3\mathcal{W}}{\partial F^3}(F_*)(\nabla\dot{\varphi}_{n+1}+\nabla\dot{\varphi}_n)^3,
\end{aligned}$$

for a constant $0\leq c\leq 1/8$ (from lemma 1) and an unknown matrix F_*. Concerning the compression term:

$$\begin{aligned}
&\frac{1}{2}\left(p_n\ \ cof\ F_n+p_{n+1}\ \ cof\ F_{n+1}\right):(F_{n+1}-F_n),\\
&=\frac{1}{2}\frac{p_n+p_{n+1}}{2}\left(cof\ F_n+cof\ F_{n+1}\right):(F_{n+1}-F_n)\\
&\quad+\frac{1}{2}\frac{p_{n+1}-p_n}{2}\left(cof\ F_{n+1}-cof\ F_n\right):(F_{n+1}-F_n),\\
&=\frac{p_n+p_{n+1}}{2}\left(\det F_{n+1}-\det F_n\right)\\
&\quad+c\,\frac{p_n+p_{n+1}}{2}\frac{\partial^3\det F}{\partial F^3}(F_{n+1}-F_n)^3\\
&\quad+\frac{1}{2}\frac{p_{n+1}-p_n}{2}\left(cof\ F_{n+1}-cof\ F_n\right):(F_{n+1}-F_n),
\end{aligned}$$

with $0\leq c\leq 1/8$. Moreover, if the initial kinematic constraint holds:

$$\int_\Omega q\left(\det\nabla\varphi_0-1+\epsilon p_0\right)=0,\quad\forall q\in\mathcal{P},$$

then, from (11, 13), it holds at every discrete time. Then, using (11), we get:

$$\int_\Omega\frac{p_n+p_{n+1}}{2}\left(\det F_{n+1}-\det F_n\right)=\epsilon\int_\Omega\frac{p_n+p_{n+1}}{2}(p_{n+1}-p_n)=\frac{\epsilon}{2}\int_\Omega(p_{n+1}^2-p_n^2).$$

After integration over Ω, we then have:

$$\begin{aligned}
&\int_\Omega\frac{1}{2}\left(p_n\ \ cof\ F_n+p_{n+1}\ \ cof\ F_{n+1}\right):(F_{n+1}-F_n)\\
&=\int_\Omega\epsilon\frac{p_{n+1}^2-p_n^2}{2}\\
&\quad+\frac{c}{8}\Delta t_n^3\frac{p_n+p_{n+1}}{2}\frac{\partial^3\det F}{\partial F^3}\left(\nabla\dot{\varphi}_n+\nabla\dot{\varphi}_{n+1}\right)^3\\
&\quad+\frac{\Delta t_n^3}{2}\frac{p_{n+1}-p_n}{2\Delta t_n}\frac{\partial^2\det F}{\partial F^2}(F_*)(\nabla\dot{\varphi}_n+\nabla\dot{\varphi}_{n+1})^2,
\end{aligned}$$

and the announced result holds:

$$\mathcal{E}_{n+1}-\mathcal{E}_n=\mathfrak{P}_n+c_n\Delta t_n^3,$$

with:

$$c_n = \alpha \frac{\partial^3 \mathcal{W}}{\partial F^3}(F_*)(\nabla\dot\varphi_{n+1}+\nabla\dot\varphi_n)^3+\beta\frac{p_n+p_{n+1}}{2}\frac{\partial^3 \det F}{\partial F^3}\left(\nabla\dot\varphi_n+\nabla\dot\varphi_{n+1}\right)^3$$
$$-\frac{1}{4}\frac{p_{n+1}-p_n}{\Delta t_n}\frac{\partial^2 \det F}{\partial F^2}(F_*)(\nabla\dot\varphi_n+\nabla\dot\varphi_{n+1})^2.$$

(2) Angular momentum evolution. If $\Gamma_D = \emptyset$, taking $v = a\times\dfrac{\varphi_n+\varphi_{n+1}}{2} = \mathbb{J}_a\cdot\dfrac{\varphi_n+\varphi_{n+1}}{2}$ in (11), the elastic term becomes:

$$\begin{aligned}
&\frac{1}{2}\left(\frac{\partial\hat{\mathcal{W}}}{\partial F}(F_n)+\frac{\partial\hat{\mathcal{W}}}{\partial F}(F_{n+1})\right)\cdot(F_n+F_{n+1})^t:\mathbb{J}_a\Delta t_n\\
&=\left(F_n\cdot\frac{\partial\mathcal{W}}{\partial C}(C_n)+F_{n+1}\cdot\frac{\partial\mathcal{W}}{\partial C}(C_{n+1})\right)\cdot(F_n+F_{n+1})^t:\mathbb{J}_a\Delta t_n,\\
&=\frac{1}{2}(F_n+F_{n+1})\cdot\left(\frac{\partial\mathcal{W}}{\partial C}(C_n)+\frac{\partial\mathcal{W}}{\partial C}(C_{n+1})\right)\cdot(F_n+F_{n+1})^t:\mathbb{J}_a\Delta t_n\\
&\quad+\frac{1}{2}(F_{n+1}-F_n)\cdot\left(\frac{\partial\mathcal{W}}{\partial C}(C_{n+1})-\frac{\partial\mathcal{W}}{\partial C}(C_n)\right)\cdot(F_n+F_{n+1})^t:\mathbb{J}_a\Delta t_n,
\end{aligned}$$

with a similar expression for the compression term in p_n. The first term vanishes because of the skew-symmetry of $\mathbb{J}_a$, but not the second which leads to an error term given by:

$$\begin{aligned}
&\Delta t_n^2\left(\nabla V_{n+1/2}\right)\cdot\left(\frac{\partial^2\mathcal{W}}{\partial C^2}(C_*):(C_{n+1}-C_n)\right)\cdot F^t_{n+1/2}:\mathbb{J}_a,\\
&=\Delta t_n^2\left(\nabla V_{n+1/2}\right)\cdot\left(\frac{\partial^2\mathcal{W}}{\partial C^2}(C_*):\left(F^t_{n+1/2}\cdot(F_{n+1}-F_n)\right)\right)\cdot F^t_{n+1/2}:\mathbb{J}_a,\\
&=\Delta t_n^3\left(\nabla V_{n+1/2}\right)\cdot\left(\frac{\partial^2\mathcal{W}}{\partial C^2}(C_*):\left(F^t_{n+1/2}\cdot\nabla V_{n+1/2}\right)\right)\cdot F^t_{n+1/2}:\mathbb{J}_a,
\end{aligned}$$

where we have denoted $V_{n+1/2} = (\dot\varphi_n+\dot\varphi_{n+1})/2$ and $F_{n+1/2} = (F_n + F_{n+1})/2$. □

In the previous proof, we have used the simple lemma (see [31] for a proof):

Lemma 1 *If $J\in\mathcal{C}^3(\mathbb{R}^{3\times3})$, then for all $F_n, F_{n+1}\in\mathbb{R}^{3\times3}$, there exists a constant $0\le c\le 1/8$ and a matrix $F_*\in\mathbb{R}^{3\times3}$ such that:*

$$J(F_{n+1}) = J(F_n)+\frac{1}{2}\left(\frac{\partial J}{\partial F}(F_n)+\frac{\partial J}{\partial F}(F_{n+1})\right):(F_{n+1}-F_n)-c\frac{\partial^3 J}{\partial F^3}(F_*)(F_{n+1}-F_n)^3.$$

Remark 2 *The above analysis underlines some key points of the trapezoidal scheme:*

- *In the compressible case, exact energy conservation is achieved only if $\hat{\mathcal{W}}$*

is a quadratic elastic potential as a function of F. It is easy to check that angular momentum is then also conserved. Nevertheless, this assumption is not realistic because incompatible with the zero volume limit ([32] page 170):

$$\lim_{\det F \to 0} \hat{\mathcal{W}}(F) \to +\infty.$$

- *Energy and angular momentum conservations are achieved with an error term $c_n \Delta t^3$, and the dependance of c_n with respect to the approximate solution is quite regular. Nevertheless, an accretive behavior (local increase of energy or/and momentum) cannot be excluded for nonlinear problems with large time steps and is indeed observed in practice, entailing numerical instability.*

3.3 Midpoint scheme

When approximating the integrals in (12) by the midpoint rule, we get the so-called midpoint scheme, corresponding to the choice:

$$\begin{cases} \Pi_{n+1/2} = \dfrac{\partial \hat{\mathcal{W}}}{\partial F}\left(\dfrac{F_n + F_{n+1}}{2}\right) - \dfrac{p_n + p_{n+1}}{2}\, cof\left(\dfrac{F_n + F_{n+1}}{2}\right), \\ D_{n+1/2} = \det\left(\dfrac{F_n + F_{n+1}}{2}\right). \end{cases} \tag{17}$$

In other words, it is a strain averaging scheme, for which we have:

Proposition 3 *The midpoint scheme achieves the following discrete evolution properties:*

(1) Discrete energy. *For a constant time step Δt,*

$$\mathcal{E}_{n+1} - \mathcal{E}_n = \mathfrak{P}_n + c_n \Delta t^3. \tag{18}$$

Here, c_n depends on the approximate solution at times n and $n+1$, but also of the discrete third order time derivative of acceleration: $\dddot{\varphi}_{n+1/2} = \frac{1}{2\Delta t^2}(\dot{\varphi}_{n+2} - \dot{\varphi}_{n+1} - \dot{\varphi}_n + \dot{\varphi}_{n+1})$.

(2) Discrete linear and angular momenta. *If $\Gamma_D = \emptyset$,*

$$\mathcal{J}_{n+1} - \mathcal{J}_n = \mathfrak{M}_n, \qquad \mathcal{I}_{n+1} - \mathcal{I}_n = \mathfrak{F}_n. \tag{19}$$

Proof : It is quite similar to the trapezoidal rule, with an exact conservation of the angular momentum conservation, due to the symmetry of the product $\Pi_{n+1/2} \cdot (F_n + F_{n+1})^t$ (see [31] for more details). The main difficulty comes from the nonlinear kinematic constraint which is poorly handled by the midpoint scheme. We denote $\square_{n+1/2} = \frac{1}{2}(\square_n + \square_{n+1})$ and $\frac{1}{2}(\dot{\square}_n + \dot{\square}_{n+1}) =$

$\frac{1}{\Delta t_n}(\square_{n+1}-\square_n)$. We assume that the step time is a constant Δt, and introduce the interpolated displacement:

$$\overline{\varphi}_{n+1/2} = \frac{1}{2}(\varphi_{n+3/2} + \varphi_{n-1/2}) = \frac{1}{4}(\varphi_{n+2} + \varphi_{n+1} + \varphi_n + \varphi_{n-1}).$$

Then, one obtains:

$$\begin{aligned}\overline{\varphi}_{n+1/2} - \varphi_{n+1/2} &= \frac{1}{4}(\varphi_{n+2} - \varphi_{n+1} - \varphi_n + \varphi_{n-1}) \\ &= \frac{\Delta t}{8}(\dot{\varphi}_{n+2} + \dot{\varphi}_{n+1} - \dot{\varphi}_n - \dot{\varphi}_{n-1}) \\ &= \frac{\Delta t^2}{4}(\ddot{\varphi}_{n+1} + \ddot{\varphi}_n),\end{aligned}$$

with $\ddot{\varphi}_n = \frac{\dot{\varphi}_{n+1}-\dot{\varphi}_{n-1}}{2\Delta t}$. The increase of displacement is defined by:

$$\begin{aligned}\delta = \varphi_{n+3/2} - \varphi_{n-1/2} &= \frac{1}{2}(\varphi_{n+2} + \varphi_{n+1} - \varphi_n - \varphi_{n-1}) \\ &= \frac{1}{2}(\dot{\varphi}_{n+3/2}\Delta t + \dot{\varphi}_{n-1/2}\Delta t + 2\varphi_{n+1} - 2\varphi_n) \\ &= 2\dot{\varphi}_{n+1/2}\Delta t + \frac{1}{2}\dddot{\varphi}_{n+1/2}\Delta t^3.\end{aligned} \tag{20}$$

By Taylor's expansion, one gets:

$$\det F_{n+3/2} - \det F_{n-1/2} = \left(cof\ \nabla\overline{\varphi}_{n+1/2}\right) : (\nabla\delta) + \frac{1}{24}\frac{\partial^2\ cof\ F}{\partial F^2}(F_*)(\nabla\delta)^3,$$

and the kinematic constraint at half time step provides:

$$\det F_{n+3/2} - \det F_{n-1/2} = -\epsilon\left(p_{n+3/2} - p_{n-1/2}\right),$$

from which we infer:

$$\left(cof\ \nabla\overline{\varphi}_{n+1/2}\right) : (\nabla\delta) = -\epsilon\left(p_{n+3/2} - p_{n-1/2}\right) - \frac{1}{24}\frac{\partial^2\ cof\ F}{\partial F^2}(F_*)(\nabla\delta)^3. \tag{21}$$

The work of pressure forces is therefore:

$$\begin{aligned}&p_{n+1/2}\ cof\ F_{n+1/2} : \nabla\dot{\varphi}_{n+1/2} = \\ &p_{n+1/2}\left(cof\ \nabla\overline{\varphi}_{n+1/2} + \frac{\partial\ cof\ F}{\partial F}(F_{**}) : \left(F_{n+1/2} - \nabla\overline{\varphi}_{n+1/2}\right)\right) : \nabla\dot{\varphi}_{n+1/2} = \\ &p_{n+1/2}\left(cof\ \nabla\overline{\varphi}_{n+1/2} - \frac{\partial\ cof\ F}{\partial F}(F_{**}) : \left(\frac{1}{4}(\nabla\ddot{\varphi}_{n+1} + \nabla\ddot{\varphi}_n)\Delta t^2\right)\right) : \nabla\dot{\varphi}_{n+1/2}.\end{aligned}$$

Since $\dot{\varphi}_{n+1/2} = \dfrac{\delta}{2\Delta t} - \dfrac{\Delta t^2}{4}\dddot{\varphi}_{n+1/2}$, we have:

$$\begin{aligned} p_{n+1/2}\, cof\, F_{n+1/2} : \nabla\dot{\varphi}_{n+1/2} = & \frac{1}{2\Delta t} p_{n+1/2} \left(cof\, \nabla\overline{\varphi}_{n+1/2} \right) : (\nabla\delta) \\ & - \frac{\Delta t^2}{4} p_{n+1/2} \left(cof\, \nabla\overline{\varphi}_{n+1/2} \right) : \nabla\ddot{\varphi}_{n+1/2} \\ & - \frac{\Delta t^2}{4} \frac{\partial\, cof\, F}{\partial F}(F_{**}) : (\nabla\ddot{\varphi}_{n+1} + \nabla\ddot{\varphi}_n) : \nabla\dot{\varphi}_{n+1/2}. \end{aligned}$$

The two last terms are of order 2 in Δt. To tackle the first one, we use (21) and up to a second order term in Δt, we get:

$$\begin{aligned} \frac{1}{2} p_{n+1/2}\, cof\, F_{n+1/2} : \nabla\dot{\varphi}_{n+1/2} = & -\frac{\Delta t^2}{48} p_{n+1/2} \frac{\partial^2\, cof\, F}{\partial F^2}(F_*)(\nabla\frac{\delta}{\Delta t})^3 \\ & - \frac{\epsilon}{2\Delta t}\, p_{n+1/2} \left(p_{n+3/2} - p_{n-1/2} \right) + O(\Delta t^2). \end{aligned}$$

By rewriting (20) for the quantity $p_{n+3/2} - p_{n-1/2}$, we finally have the expected evolution of energy:

$$\Delta t\; p_{n+1/2}\, cof\, F_{n+1/2} : \nabla\dot{\varphi}_{n+1/2} = \frac{\epsilon}{2}(p_{n+1}^2 - p_n^2) + O(\Delta t^3),$$

up to a third order term in Δt. □

Remark 3 *The midpoint scheme has the following key characteristics:*

- *This scheme is known to be symplectic in the compressible framework (see [9,10,33]). For small time steps, a backward analysis (see [9]) proves conservation of a discrete energy which is equal to the physical one up to a $O(\Delta t^2)$ term. Nevertheless, the time steps used in practice may be too large to ensure such a property in real applications. Moreover, symplecticity is hard to obtain for constrained problems (see [11]); in particular, it is lost in the incompressible framework.*
- *For compressible materials with (unrealistic) quadratic elastic potential $\hat{\mathcal{W}}$, energy would be exactly conserved.*
- *Writing the nonlinear kinematic constraint at midpoint has bad consequences on energy conservation. In particular, it requires a very high regularity in time for the solution.*
- *Angular and linear momenta are exactly conserved. The scheme respects rotations and translations.*

A few conclusions can be drawn from the above analysis, stated here for the incompressible case (see also [2]):

- The better conservation of energy achieved by the trapezoidal rule in comparison with the midpoint scheme, is due to the imposition of the kinematic constraint at entire time steps, rather than at midtime steps. In (11), it is then natural to adopt:

$$D_{n+1/2} = \frac{1}{2}\left(\det F_n + \det F_{n+1}\right). \tag{22}$$

- The exact conservation of momenta performed by the midpoint scheme is due to the natural form of the first algorithmic stress tensor:

$$\Pi_{n+1/2} = \left(\frac{F_n + F_{n+1}}{2}\right) \cdot \Sigma_{n+1/2}, \tag{23}$$

  with a symmetric second stress tensor $\Sigma_{n+1/2}$.
- Then, with such a construction of $\Pi_{n+1/2}$, it is straightforward (see [2]) to check that exact energy conservation is achieved if and only if we can satisfy:

$$\frac{1}{2}\int_\Omega \Sigma_{n+1/2} : (C_{n+1} - C_n) = \int_\Omega \left(\mathcal{W}(C_{n+1}) + \frac{\epsilon}{2}p_{n+1}^2\right) - \int_\Omega \left(\mathcal{W}(C_n) + \frac{\epsilon}{2}p_n^2\right). \tag{24}$$

A major goal is then to construct such a tensor $\Sigma_{n+1/2}$ satisfying (24). A first possibility has been proposed by Simo and Tarnow [2]. In the quasi-incompressible case, this would yield:

$$\begin{aligned}\Sigma_{n+1/2} := &\left(\frac{\partial \mathcal{W}}{\partial C}(\beta_n C_n + (1-\beta_n)C_{n+1}) + \frac{\partial \mathcal{W}}{\partial C}((1-\beta_n)C_n + \beta_n C_{n+1})\right) \\ &- \frac{p_n + p_{n+1}}{2}\left(\frac{\partial \det C^{1/2}}{\partial C}(\gamma_n C_n + (1-\gamma_n)C_{n+1})\right. \\ &\left. + \frac{\partial \det C^{1/2}}{\partial C}((1-\gamma_n)C_n + \gamma_n C_{n+1})\right),\end{aligned} \tag{25}$$

with constants β_n and γ_n to be computed at each time step and at each Gauss point such that (24) holds. Such an approach, consisting of a local averaging of the stresses, has been implemented by [4], and shares features with the recent work [5] in which stresses are integrated over a linear interpolation of the strain tensor.

An exact stress-averaging [5] or the somewhat equivalent determination of the weights β_n,γ_n in (25) is avoided by the following explicit expression from Gon-

zalez [3], which can be generalized to quasi-incompressible models by setting:

$$\begin{aligned}\Sigma_{n+1/2} := & 2\frac{\partial \mathcal{W}}{\partial C}(C_{n+1/2}) \\ & +2\left(\mathcal{W}(C_{n+1}) - \mathcal{W}(C_n) - \frac{\partial \mathcal{W}}{\partial C}(C_{n+1/2}) : \delta C_n\right)\frac{\delta C_n}{\delta C_n : \delta C_n} \\ & -(p_n + p_{n+1})\left[\frac{\partial \det C^{1/2}}{\partial C}(C_{n+1/2}) + \right. \\ & \left. +\left(\det C_{n+1}^{1/2} - \det C_n^{1/2} - \frac{\partial \det C^{1/2}}{\partial C}(C_{n+1/2}) : \delta C_n\right)\frac{\delta C_n}{\delta C_n : \delta C_n}\right],\end{aligned} \tag{26}$$

with $C_{n+1/2} = \frac{1}{2}(C_n + C_{n+1})$, and $\delta C_n = C_{n+1} - C_n$.

Remark 4 *At the limit $\delta C_n \to 0$, the stress tensor proposed in (26) behaves like*

$$\Sigma_{n+1/2} = 2\frac{\partial \mathcal{W}}{\partial C}(C_{n+1/2}) + \frac{1}{12}\frac{\partial^3 \mathcal{W}}{\partial C^3}(C_{n+1/2})\delta C_n^3 \frac{\delta C_n}{\|\delta C_n\|^2} + o(\|\delta C_n\|^4),$$

which shows that the proposed correction is second order in δC_n. As pointed at by [5], the expression (26) may seem less natural than a local averaging, and introduce some anisotropy, but the above expansion shows local equivalence in time up to a second order error term. Moreover, the apparently complex correction term introduced in (26) represents the error between the derivative of $\mathcal{W}$ and its finite difference approximation along the increment of strains.

In the hyperelastic framework, one can use indifferently as $\Sigma_{n+1/2}$ the expressions provided by [2],[5] or [3]. Nevertheless, in the extensions of section 5, we specifically adapt the energy correction proposed in [3].

Proposition 4 *By construction, the expression of $\Sigma_{n+1/2}$ given by (26) satisfies (24). Thus, the time integration scheme (11), with $\Pi_{n+1/2}$, $D_{n+1/2}$ and $\Sigma_{n+1/2}$ respectively given by (23), (22) and (26), known as the Gonzalez scheme [3], preserves energy, angular and linear momenta.*

Remark 5 *In a Newton's method, nonlinear problems are solved by successive linearizations. Here, the linearized time integrator is not symmetric, which is a noticeable complication. An interesting idea, already mentioned in [21], is to decompose the proposed stress into:*

$$\Sigma_{n+1/2} = 2\frac{\partial \mathcal{W}}{\partial C}(C(\varphi_{n+1/2})) + \underbrace{\left(\Sigma_{n+1/2} - 2\frac{\partial \mathcal{W}}{\partial C}(C(\varphi_{n+1/2}))\right)}_{(\dagger)},$$

where $C(\varphi_{n+1/2}) = \nabla^t \varphi_{n+1/2} \cdot \nabla \varphi_{n+1/2}$ is the midpoint right Cauchy-Green strain tensor, and in which the second order correction term denoted by (†) is not taken into account into the Newton jacobian matrix. The disadvantage of the proposed quasi-Newton methods is a non-quadratic convergence, but the practical overcost is almost negligible.

Remark 6 *As observed in (26), energy correction has to be applied on all components of the stress tensor, including those induced by the nonlinear kinematic constraints. Adding new features such as contact or viscoelasticity will require more energy correction terms, as observed later in section 5.*

4 Energy-dissipative schemes

4.1 Conservation analysis for the HHT scheme

In linear elastodynamics, it is useful for stability reasons to use schemes whose spectral radius r is strictly less than 1 because:

(1) possible polynomial instabilities are avoided (arising when $r = 1$ in presence of a multiple unit eigenvalue),
(2) information is dissipated at highest frequencies, which are not properly resolved at the numerical level,
(3) the condition number of the linear systems to be solved is improved,
(4) there exist a quadratic form whose value diminishes along the discrete evolution (Liapunov L-asymptotic stability).

A good example is the popular second order Hilber-Hughes-Taylor (HHT) scheme. We present here a nonlinear analysis of this scheme, showing that the above advantages are no more conserved in a nonlinear framework. Nevertheless, it is the occasion to show that in the linear framework, the scheme is strictly dissipative for a modified energy and to propose a modification of Gonzalez energy-conserving scheme [3] (reviewed and generalized in (26)) which respects such a dissipation property in a nonlinear framework.

For a given $\alpha \geq 0$, the natural extension of the HHT scheme [1,34] to nonlinear elastodynamics is given by:

$$\begin{cases} \displaystyle\int_\Omega \rho \ddot{\varphi}_{n+1} \cdot v + \int_\Omega (\alpha \Pi_n + (1-\alpha)\Pi_{n+1}) : \nabla v = \int_\Omega f_{n+1-\alpha} \cdot v + \int_{\Gamma_N} g_{n+1-\alpha} \cdot v, \\ \displaystyle\int_\Omega q \,(\det F_{n+1} - 1) = 0, \end{cases} \tag{27}$$

for all $v \in \mathcal{U}_0$ and $q \in \mathcal{P}$, where displacement, velocity and acceleration fields are related through Newmark's relations:

$$\begin{cases} \dot{\varphi}_{n+1} - \dot{\varphi}_n = \Delta t_n \left(\left(\frac{1}{2} - \alpha \right) \ddot{\varphi}_n + \left(\frac{1}{2} + \alpha \right) \ddot{\varphi}_{n+1} \right), \\ \varphi_{n+1} - \varphi_n = \Delta t_n \frac{\dot{\varphi}_n + \dot{\varphi}_{n+1}}{2} + \frac{\alpha^2 \Delta t_n^2}{4} \left(\ddot{\varphi}_{n+1} - \ddot{\varphi}_n \right). \end{cases} \tag{28}$$

The notation $\square_{n+1-\alpha}$ classically stands for $\alpha \square_n + (1-\alpha)\square_{n+1}$.

In the linearized case, we recall from [1,34] that the present scheme has a spectral radius which is strictly smaller than unity for any $\alpha > 0$. In the nonlinear framework, we prove

Proposition 5 *Assume for simplicity that the time step is constant. Then, the nonlinear HHT scheme (27) achieves the following discrete evolution properties:*

(1) Discrete energy. *Up to higher order terms depending only of time variations in force, we have:*

$$\mathcal{E}_{n+1}^{\alpha} - \mathcal{E}_n^{\alpha} = \mathfrak{P}_n - \mathfrak{D}_n^{\alpha} \Delta t^2 + c_n \Delta t^3, \tag{29}$$

where the discrete energy $\mathcal{E}_n^{\alpha}$ is defined by

$$\mathcal{E}_n^{\alpha} = \mathcal{E}_n + \frac{\alpha^2 \, \Delta t^2}{8} \int_{\Omega} \rho \ddot{\varphi}_n^2,$$

and c_n is defined as for the trapezoidal rule and depends on displacements and pressures at times n and $n+1$, on the approximate velocity $V_{n+1/2} = \frac{1}{\Delta t}(\varphi_{n+1} - \varphi_n)$, and on the approximate pressure time derivative $\pi_{n+1/2} = \frac{1}{\Delta t}(p_{n+1} - p_n)$. The coefficient $\mathfrak{D}_n^{\alpha}$ has the following expression:

$$\begin{aligned} \mathfrak{D}_n^{\alpha} = {} & \frac{\alpha^3}{4} \int_{\Omega} \rho \left(\ddot{\varphi}_{n+1} - \ddot{\varphi}_n \right)^2 \\ & + k \Delta t_n \int_{\Omega} \ddot{\Pi}_n : (\nabla V_{n+1/2}) - k \Delta t_n \int_{\Omega} \frac{\partial^2 f}{\partial t^2}(t_n) \cdot V_{n+1/2}, \end{aligned}$$

where $\ddot{\Pi}_n$ is the centered second order finite difference:

$$\ddot{\Pi}_n = \frac{1}{\Delta t^2} \left(\Pi_{n-1} - 2\Pi_n + \Pi_{n+1} \right) = \frac{1}{\Delta t} \left(\dot{\Pi}_{n+1/2} - \dot{\Pi}_{n-1/2} \right).$$

(2) Discrete angular momentum. *Up to higher order terms, we have:*

$$\mathcal{J}_{n+1} - \mathcal{J}_n = \mathfrak{M}_n + c_n \Delta t^3, \tag{30}$$

where c_n depends on the approximate solution at times $n-1$, n and $n+1$, on the accelerations $\ddot{\varphi}_{n-1}$, $\ddot{\varphi}_n$ et $\ddot{\varphi}_{n+1}$, and on the approximate second order time derivative $\frac{1}{\Delta t}(\pi_{n+1/2} - \pi_{n-1/2})$.

(3) Discrete linear momentum. *Up to higher order terms depending only of the time variations in force, we have:*

$$\mathcal{I}_{n+1} - \mathcal{I}_n = \mathfrak{F}_n + c_n \Delta t^3, \tag{31}$$

where c_n only depends on the second order time derivative of f.

Proof : In order to simplify the expressions to come, we assume that the surface load g is zero. A linear combination of the discrete systems at times n and $n+1$, with respective coefficients $(1-\gamma) = \frac{1}{2} - \alpha$ and $\gamma = \frac{1}{2} + \alpha$ gives:

$$\begin{aligned}
&\int_\Omega \rho \frac{\dot{\varphi}_{n+1} - \dot{\varphi}_n}{\Delta t_n} \cdot v + \int_\Omega \underbrace{k\left(\Pi_{n-1} - 2\Pi_n + \Pi_{n+1}\right)}_{\aleph_n} : \nabla v + \int_\Omega \frac{\Pi_n + \Pi_{n+1}}{2} : \nabla v = \\
&\int_\Omega \frac{f_n + f_{n+1}}{2} \cdot v + \int_\Omega \underbrace{k\left(f_{n-1} - 2f_n + f_{n+1}\right)}_{\mathfrak{f}_n} \cdot v,
\end{aligned} \tag{32}$$

in which $k = \alpha(\frac{1}{2} - \alpha) > 0$ for $0 \leq \alpha \leq \frac{1}{2}$. The form (32),(28) of the scheme adds to the trapezoidal rule some "correction terms". We only detail these additional contributions.

(1) Energy evolution. By using $v = (\varphi_{n+1} - \varphi_n)$ in (32), and the relations (28), the inertial term takes the form:

$$\begin{aligned}
&\int_\Omega \rho \frac{\dot{\varphi}_{n+1} - \dot{\varphi}_n}{\Delta t_n} \cdot v = \int_\Omega \rho(\dot{\varphi}_{n+1} - \dot{\varphi}_n) \cdot \frac{\dot{\varphi}_n + \dot{\varphi}_{n+1}}{2} \\
&+\Delta t_n^2 \frac{\alpha^2}{4} \int_\Omega \rho \left((\frac{1}{2} - \alpha)\ddot{\varphi}_n + (\frac{1}{2} + \alpha)\ddot{\varphi}_{n+1} \right) \cdot (\ddot{\varphi}_{n+1} - \ddot{\varphi}_n), \\
=& \frac{1}{2} \int_\Omega \rho \dot{\varphi}_{n+1}^2 - \frac{1}{2} \int_\Omega \rho \dot{\varphi}_n^2 \\
&+\Delta t_n^2 \frac{\alpha^2}{8} \int_\Omega \rho \left(\ddot{\varphi}_{n+1}^2 - \ddot{\varphi}_n^2 \right) + \Delta t_n^2 \frac{\alpha^3}{4} \int_\Omega \rho \left(\ddot{\varphi}_{n+1} - \ddot{\varphi}_n \right)^2.
\end{aligned} \tag{33}$$

The non-trapezoidal contribution to the stress terms is by construction

$$\int_\Omega \aleph_n : \nabla v = k \Delta t^3 \int_\Omega \ddot{\Pi}_n : (\nabla V_{n+1/2}).$$

Concerning corrections on the force term, we have

$$\int_\Omega \mathfrak{f}_n \cdot v = k \Delta t^3 \int_\Omega \frac{\partial^2 f}{\partial t^2}(t_n) \cdot V_{n+1/2} + o(\Delta t^3).$$

As a consequence, up to higher orders in Δt concerning only the variations of f, we obtain:

$$\mathcal{E}^{\alpha}_{n+1} - \mathcal{E}^{\alpha}_{n} = \mathfrak{P}_n - \mathfrak{D}^{\alpha}_{n}\Delta t_n^2 + c_n \Delta t_n^3,$$

with:

$$\begin{aligned}\mathfrak{D}^{\alpha}_{n} = & \frac{\alpha^3}{4}\int_\Omega \left(\ddot{\varphi}_{n+1} - \ddot{\varphi}_n\right)^2 \\ & + k\Delta t \int_\Omega \ddot{\Pi}_n : (\nabla V_{n+1/2}) - k\Delta t \int_\Omega \frac{\partial^2 f}{\partial t^2}(t_n)\cdot V_{n+1/2}.\end{aligned}$$

(2) Angular and linear momenta evolutions. Assuming that $\Gamma_D = \emptyset$, we use $v = \Delta t\, \mathbb{J}_a \cdot \frac{\varphi_n + \varphi_{n+1}}{2}$ in (32). The non-trapezoidal contribution of stresses is:

$$\Delta t \int_\Omega \aleph_n \cdot \left(\frac{F_n + F_{n+1}}{2}\right)^t : \mathbb{J}_a = k\Delta t^3 \int_\Omega \ddot{\Pi}_n \cdot \left(\frac{F_n + F_{n+1}}{2}\right)^t : \mathbb{J}_a$$

which is clearly third order in Δt, with a similar expression for the terms in $\mathfrak{f}_n$. The case of linear momentum is similar using constant fields of displacements v in (32).

□

Remark 7 *To recover the stability properties of the linear case, we can apply the above result by assuming that $\hat{\mathcal{W}}$ is quadratic as a function of F, and that the incompressibility constraint is linear. Then:*

$$\int_\Omega \Pi : \nabla v = \int_\Omega \frac{\partial \hat{\mathcal{W}}}{\partial F} : \nabla v - p\, div\, v, \quad \forall v \in \mathcal{U}_0, \qquad \epsilon p = -\, div(\varphi - id).$$

In this case, we have $c_n = 0$ because the trapezoidal rule is energy-conserving, and assume here that $f = 0$. Since:

$$\begin{aligned}F_{n+1} - F_n = & \frac{1}{2}\left(F_{n+1} - F_n\right) + \frac{1}{2}\left(F_n - F_{n-1}\right) \\ & + \frac{1}{2}\left(F_{n+1} - F_n\right) - \frac{1}{2}\left(F_n - F_{n-1}\right), \\ \Delta t^2 \ddot{\Pi}_n = & \left(\Pi_{n+1} - \Pi_n\right) - \left(\Pi_n - \Pi_{n-1}\right), \end{aligned} \tag{34}$$

we have

$$\begin{aligned}\Delta t^3\ \ddot{\Pi}_n : \nabla V_{n+1/2} &= \Delta t^2 \ddot{\Pi}_n : (F_{n+1} - F_n) \\ &= \hat{\mathcal{W}}\,(F_{n+1} - F_n) - \hat{\mathcal{W}}\,(F_n - F_{n-1}) \\ &\quad + \frac{\epsilon}{2}(p_{n+1} - p_n)^2 - \frac{\epsilon}{2}(p_n - p_{n-1})^2 \\ &\quad + \hat{\mathcal{W}}\,(F_{n+1} - 2F_n + F_{n-1}) \\ &\quad + \frac{\epsilon}{2}\,(p_{n+1} - 2p_n + p_{n-1})^2\,.\end{aligned}$$

Then, the following modified quadratic energy:

$$\begin{aligned}&\mathcal{E}_n^{HHT} = \frac{1}{2}\int_\Omega \rho\dot{\varphi}_n^2 + \int_\Omega \hat{\mathcal{W}}(F_n) + \frac{\epsilon}{2}\int_\Omega p_n^2 \\ &+\frac{\alpha^2\Delta t^2}{8}\int_\Omega \rho\ddot{\varphi}_{n+1}^2 + k\Delta t^2\hat{\mathcal{W}}\left(\dot{F}_{n-1/2}\right) + \frac{k\epsilon}{2}\Delta t^2(\dot{p}_{n-1/2})^2,\end{aligned}$$

decreases with time. More precisely, we have:

$$\begin{aligned}&\mathcal{E}_{n+1}^{HHT} - \mathcal{E}_n^{HHT} = -\frac{\alpha^3\Delta t^2}{4}\int_\Omega \rho\,(\ddot{\varphi}_{n+1} - \ddot{\varphi}_n)^2 \\ &-k\Delta t^4\int_\Omega \hat{\mathcal{W}}\left(\ddot{F}_n\right) - \frac{k\epsilon}{2}\Delta t^4\,(\ddot{p}_n)^2 \le 0,\end{aligned}$$

with obvious notation for $\dot{F}_{n-1/2} = (F_n - F_{n-1})/\Delta t$, $\dot{p}_{n-1/2} = (p_n - p_{n-1})/\Delta t$, $\ddot{F}_n$ *and* $\ddot{p}_n$*. Therefore, for linear elastodynamics, there exists a quadratic form* $\mathcal{E}_n^{HHT}$ *diminishing along the HHT discrete evolution. This confirms the fact that the spectral radius of the time integrator is less than one. Nevertheless, this quadratic form does not coincide with the usual mechanical energy. It introduces acceleration terms in the energy and high order terms in time in the dissipation, which are larger for larger frequencies.*

Remark 8 • *Groups of symmetry are not well preserved by the discrete dynamics as momenta are not conserved. This remark confirms the work of Armero and Romero in [20]; they prove the non-existence of relative equilibria for the HHT discrete dynamics in the case of a nonlinear spring-mass system.*

- *In a nonlinear framework, we can no longer control the sign of* $\mathfrak{D}_n^\alpha$*, and therefore this term cannot be interpreted as a dissipation term.*

4.2 A new dissipative scheme in the nonlinear framework

The previous analysis leads us to propose a modified dissipative scheme by using a second order non-trapezoidal Newmark time integration of the inertial

term, while keeping Gonzalez energy conserving formulation for the algorithmic Piola-Kirchhoff stress tensor at midtime. More precisely, we propose the following integration scheme:

$$\begin{cases} \displaystyle\int_\Omega \rho \left[\left(\frac{1}{2} - \alpha \right) \ddot{\varphi}_n + \left(\frac{1}{2} + \alpha \right) \ddot{\varphi}_{n+1} \right] \cdot v + \int_\Omega \Pi_{n+1/2} : \nabla v = \\ \displaystyle\int_\Omega \frac{f_n + f_{n+1}}{2} \cdot v + \int_{\Gamma_N} \frac{g_n + g_{n+1}}{2} \cdot v, \quad \forall v \in \mathcal{U}_0, \\ \displaystyle\int_\Omega q \ (\det \nabla \varphi_{n+1} - 1 - \epsilon p_{n+1}) = 0, \quad \forall q \in \mathcal{P}, \end{cases} \tag{35}$$

where $\Pi_{n+1/2}$ is the first Piola-Kirchhoff algorithmic stress tensor proposed in (23) and (26), and where the acceleration terms are obtained from the Newmark's relations (28). Second order accuracy is ensured by taking $\alpha = \eta_\alpha \Delta t_n > 0$. Then, we obtain the following result:

Proposition 6 *The scheme (35),(28) achieves the following conservation properties:*

(1) Discrete energy.

$$\mathcal{E}^\alpha_{n+1} - \mathcal{E}^\alpha_n = \mathfrak{P}_n - \frac{\alpha^3 \Delta t_n^2}{4} \int_\Omega \rho \left(\ddot{\varphi}_{n+1} - \ddot{\varphi}_n \right)^2 \leq \mathfrak{P}_n, \tag{36}$$

with the modified energy:

$$\mathcal{E}^\alpha_n = \frac{\alpha^2 \Delta t_n^2}{8} \int_\Omega \rho \ddot{\varphi}_n^2 + \frac{1}{2} \int_\Omega \rho \dot{\varphi}_n^2 + \int_\Omega \hat{\mathcal{W}}(\nabla \varphi_n).$$

(2) Discrete angular and linear momenta. *If $\Gamma_D = \emptyset$, we have:*

$$\mathcal{J}_{n+1} - \mathcal{J}_n = \mathfrak{M}_n, \qquad \mathcal{I}_{n+1} - \mathcal{I}_n = \mathfrak{F}_n. \tag{37}$$

Proof : The proof of energy dissipation readily comes from the previous analysis of the HHT scheme, using (35) with $v = \varphi_{n+1} - \varphi_n$, which yields (33). The elastic part behaves perfectly due to the choice of a "conservative" Piola-Kirchhoff stress tensor $\Pi_{n+1/2}$. □

In a practical implementation of the present scheme, the displacements are first obtained by solving (35) after elimination of velocity and acceleration through (28), and (28) is then used to update velocity and acceleration. This requires a proper initialization of the velocity and acceleration field at the first time step, which is achieved by computing two time steps with a midpoint, a trapezoidal or any other second order conservative scheme with given initial displacements φ_0 and velocities $\dot{\varphi}_0$.

Let us finish this section by the illustration of the dissipative properties of the scheme, as a function of the frequency. Assume the forcing terms are such

that the numerical solution of the nonlinear problem is mono-frequential at pulsation ω, and can be written by separation of space and time variables as

$$\varphi_n(x) = \sin(\omega t_n)\psi(x),$$

with $\varphi_0 = 0$, $\dot{\varphi}_0 = \omega\psi$, $\ddot{\varphi}_0 = 0$, and $\int_\Omega \psi^2 = 1$. We choose $\rho = 1$ on Ω. To illustrate the spectral behavior of the scheme, we compute velocities and accelerations through relations (28) on the interval $[0, 100]$, the time step $\Delta t = 1$ being fixed. The following graph (figure 1) represents the total energy which is numerically dissipated during the time interval $[0, 100]$, i.e.

$$\mathbb{D} = \frac{\alpha^3 \Delta t^2}{4} \sum_{n=0}^{99} \int_\Omega \left(\ddot{\varphi}_{n+1} - \ddot{\varphi}_n\right)^2,$$

divided by the initial kinetic energy $\frac{1}{2}\omega^2$ as a function of $0 \leq \omega \leq \pi$ and η_α.

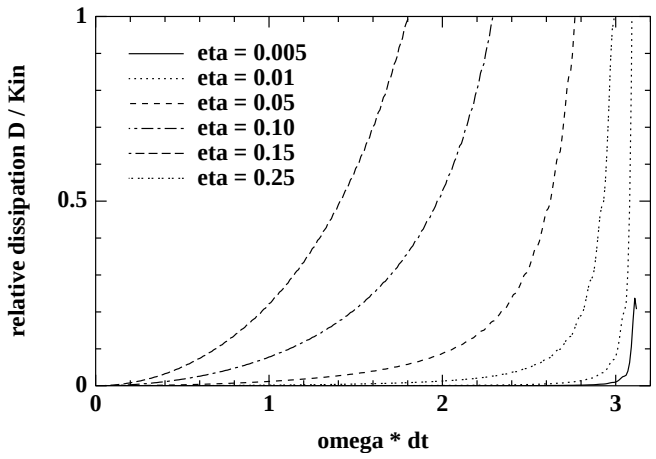

Fig. 1. The relative dissipation $2\mathbb{D}/\omega^2$ provided by the scheme as a function of ω and η_α over the interval $[0, T]$ ($T = 100$;$\Delta t = 1$); η_α being given, when ω is such that $2\mathbb{D}/\omega^2 = 1$, then the total initial kinetic energy has been dissipated during $[0, T]$. The curves increase faster for higher values of η_α.

For a value of $\eta_\alpha = 0.05$, the curve is flat at low frequencies ($\omega\Delta t < 2$), and still exhibits interesting dissipation features at higher frequencies. Assuming that discrete accelerations are consistent with their continuous counterpart of the imposed solution, $\mathbb{D}$ behaves in fact like

$$\mathbb{D} \approx \frac{\alpha^3 \Delta t^3}{4} \omega^6 \int_0^T \int_\Omega \cos^2(\omega t)\psi^2(x)\, dx\, dt.$$

5 Extensions of the conservative approach

5.1 Frictionless contact

5.1.1 Model

Let $\Omega^{(1)}$ and $\Omega^{(2)}$ be two open sets in $\mathbb{R}^3$ representing the interior of the reference configurations of two solids potentially in contact on the parts $\Gamma_C^{(i)} \subset \Gamma_N^{(i)} \subset \partial\Omega^{(i)}$ $(i \in \{1,2\})$ of their boundaries. For each solid $i \in \{1,2\}$, $\square^{(i)}$ will denote the quantity $\square$ relative to $\Omega^{(i)}$. In this presentation, $\Gamma_C^{(2)}$ will be considered as the master surface. We introduce for all $x \in \Gamma_C^{(1)}$, its closest-point projection on the deformed master surface:

$$\overline{y}(t,x) = \arg\min_{y \in \Gamma_C^{(2)}} \|\varphi^{(1)}(t,x) - \varphi^{(2)}(t,y)\|_2.$$

When $\Gamma_C^{(2)}$ is continuously differentiable, there exists a continuous scalar gap function $g : [0,T] \times \Gamma_C^{(1)} \to \mathbb{R}$ defined by

$$g(t,x) = -\left(\varphi^{(1)}(t,x) - \varphi^{(2)}(t,\overline{y}(t,x))\right) \cdot \nu(t,\overline{y}(t,x)),$$

where $\nu(t,y)$ is the normal outward unit vector to $\varphi^{(2)}(t,\Gamma_C^{(2)})$ at time $t \in [0,T]$ and point $y \in \Gamma_C^{(2)}$. By definition of the closest projection, we have:

$$\varphi^{(1)}(t,x) - \varphi^{(2)}(t,\overline{y}(t,x)) = -g(t,x)\ \nu(t,\overline{y}(t,x)),$$

and the non-penetration condition between the two solids takes the form:

$$g(t,x) \leq 0.$$

By construction, we also have

$$\frac{\partial g}{\partial \varphi^{(1)}} \cdot v^{(1)}(x) = -v^{(1)}(x)\nu(t,\overline{y}(t,x))$$
$$\frac{\partial g}{\partial \varphi^{(2)}} \cdot v^{(2)}(x) = v^{(2)}(\overline{y}(t,x))\nu(t,\overline{y}(t,x)).$$

With this notation, the weak form of the balance of linear momentum with frictionless contact reads:

$$\sum_{i=1}^{2}\int_{\Omega^{(i)}}\rho^{(i)}\ddot{\varphi}^{(i)}\cdot v^{(i)}+\int_{\Omega^{(i)}}\Pi^{(i)}:\nabla v^{(i)}=\sum_{i=1}^{2}\int_{\Omega^{(i)}}f^{(i)}\cdot v^{(i)}$$
$$+\underbrace{\int_{\Gamma_C^{(1)}}\lambda(t,x)\nu(t,\overline{y}(t,x))\cdot\Big[v^{(1)}(x)-v^{(2)}(\overline{y}(t,x))\Big]}_{G(v^{(1)},v^{(2)})}, \tag{38}$$

for all admissible virtual displacements $v^{(i)}\in\mathcal{U}_0(\Omega^{(i)})$, $i\in\{1,2\}$. The corresponding Kuhn-Tucker conditions characterizing the normal reaction force $\lambda(t,x)$ are:

$$\begin{cases}\lambda(t,x)\geq 0,\\ g(t,x)\leq 0,\\ \lambda(t,x)g(t,x)=0,\end{cases} \tag{39}$$

for almost all $(t,x)\in[0,T]\times\Omega$ (see [35]). In addtion, for energy conservation purpose, the following persistency condition (see [36]) must also be imposed:

$$\lambda(t,x)\dot{g}\left(\varphi(t,x)\right)=0. \tag{40}$$

The condition (40) means that normal contact reactions can only appear during persistent contact on the rigid surface.

5.1.2 Conservation properties in the continuous framework

The two-body system still respects the usual energy and momenta conservation properties in the absence of external forces [27]. The key-point is to observe that the work of normal contact reactions at time t vanishes:

$$\begin{aligned}G(\dot{\varphi}^{(1)}(t),\dot{\varphi}^{(2)}(t))&=-\int_{\Gamma_C}\lambda(t,x)\nu(t,\overline{y}(t,x))\cdot\Big(\dot{\varphi}^{(1)}(t,x)-\dot{\varphi}^{(2)}(t,\overline{y}(t,x))\Big)\\&=\int_{\Gamma_C}\lambda(t,x)\left(\frac{\partial g}{\partial\varphi^{(1)}}\cdot\dot{\varphi}^{(1)}(t,x)+\frac{\partial g}{\partial\varphi^{(2)}}\cdot\dot{\varphi}^{(2)}(t,x)\right)\\&=\int_{\Gamma_C}\lambda(t,x)\dot{g}(t,x)\\&=0.\end{aligned}$$

When the conditions (39) are enforced by a penalty technique, the Lagrange multiplier λ is defined as:

$$\lambda=\frac{1}{\eta}g^{+},\quad [0,T]\times\Omega,$$

with $g^{+}=g$ if $g\geq 0$ and $g^{+}=0$ otherwise. Then, the persistency condition

(40) is no more necessary and the work of contact forces takes the form:

$$\int_{\Gamma_C} \lambda(t,x)\dot{g}(t,x) = \frac{d}{dt}\left(\frac{1}{2\eta}\int_{\Gamma_C}\left(g^+\right)^2\right),$$

resulting in the absence of external forces, in the conservation of a penalized total energy of the two-body system:

$$\mathcal{E}(t) = \frac{1}{2\eta}\int_{\Gamma_C}\left(g^+(t)\right)^2 + \sum_{i=1}^{2}\mathcal{E}^{(i)}(t).$$

5.1.3 A conserving time integration approach

To reproduce in the discrete framework the previous conservation properties, we adapt the energy correction approach of [3] already employed in the previous section and propose the following midtime approximations of the normal contact force $G_{n+1/2}$, normal vector $\hat{\nu}_{n+1/2}$ and reaction intensity $\Lambda_{n+1/2}$:

$$G_{n+1/2}(v^{(1)},v^{(2)}) = \int_{\Gamma_C^{(1)}} \Lambda_{n+1/2}\hat{\nu}_{n+1/2}\cdot\left[v^{(1)}(x) - v^{(2)}(\overline{y}_{n+1/2}(x))\right], \tag{41}$$

$$\hat{\nu}_{n+1/2} = -\nu_{n+1/2} + \left[g_{n+1} - g_n + \nu_{n+1/2}\cdot\delta\varphi_n\right]\frac{\delta\varphi_n}{\delta\varphi_n\cdot\delta\varphi_n}, \tag{42}$$

$$\begin{aligned}\Lambda_{n+1/2} &= \lambda_{n+1/2} + \left[\frac{\lambda_{n+1}\,g_{n+1} - \lambda_n\,g_n}{2} - \lambda_{n+1/2}\delta g_n\right]\frac{\delta g_n}{(\delta g_n)^2},\\ &= \frac{\lambda_{n+1}\,g_{n+1} - \lambda_n\,g_n}{2\delta g_n}\\ &= \frac{1}{2}\left(\frac{\lambda_{n+1}+\lambda_n}{2} + \frac{g_{n+1}+g_n}{2\eta}\left(\frac{g^+_{n+1}-g^+_n}{g_{n+1}-g_n}\right)\right).\end{aligned} \tag{43}$$

Here $\overline{y}_{n+p}(x)$ is the projection of $\varphi^{(1)}_{n+p}(x)$ over $\varphi^{(2)}_{n+p}(\Gamma_C)$ with the notation $p = n$, $n+1/2$ or $n+1$ and :

$$\varphi^{(i)}_{n+1/2} = \frac{1}{2}\left(\varphi^{(i)}_n + \varphi^{(i)}_{n+1}\right).$$

Moreover, $\nu_{n+p}(x)$ is the normal outward unit vector to $\varphi^{(2)}_{n+p}(\Gamma^{(2)}_C)$ at point $\overline{y}_{n+p}(x) \in \Gamma^{(2)}_C$, and:

$$\begin{cases} g_n(x) = -\left(\varphi^{(1)}_n(x) - \varphi^{(2)}_n(\overline{y}_n(x))\right)\cdot\nu_n(x),\\ \delta\varphi_n(x) = \left[\varphi^{(1)}_{n+1}(x) - \varphi^{(2)}_{n+1}(\overline{y}_{n+1/2}(x))\right] - \left[\varphi^{(1)}_n(x) - \varphi^{(2)}_n(\overline{y}_{n+1/2}(x))\right],\\ \delta g_n(x) = g_{n+1}(x) - g_n(x),\\ \lambda_{n+p}(x) = g^+_{n+p}(x)/\eta. \end{cases}$$

Observe that since $\nu_{n+1/2} \cdot \delta\varphi_n = -\frac{\partial g}{\partial \varphi}(\varphi_{n+1/2}) \cdot (\varphi_{n+1} - \varphi_n)$ and $\lambda_{n+1/2}\delta g_n = \frac{\partial \lambda g/2}{\partial g}(g_{n+1/2})\delta g_n$, the above corrections in $\hat{\nu}_{n+1/2}$ and $\Lambda_{n+1/2}$ are again second order in $\delta\varphi$ and δg. Also observe that the proposed reaction force is simply the reaction average $\Lambda_{n+1/2} = \frac{\lambda_{n+1}+\lambda_n}{2}$ when the body is in contact at both times n and $n+1$, but is different from this average at the beginning and at the end of the impact. Moreover

Proposition 7 *The frictionless contact forces defined by (41) are conservative with respect to energy and linear momentum in the sense that:*

$$\begin{aligned} G_{n+1/2}(\varphi^{(1)}_{n+1} - \varphi^{(1)}_n, \varphi^{(2)}_{n+1} - \varphi^{(2)}_n) &= \frac{1}{2}\int_{\Gamma_C^{(1)}} \lambda_{n+1} g_{n+1} - \lambda_n g_n \\ &= \frac{1}{2\eta}\int_{\Gamma_C} \left(g^+_{n+1}\right)^2 - \left(g^+_n\right)^2 \qquad (44) \\ G_{n+1/2}(a,a) &= 0, \quad \forall a \in \mathbb{R}^3. \qquad (45) \end{aligned}$$

Proof : The zero resultant force is readily obtained from (41). Concerning energy, we have by construction:

$$\begin{aligned} G_{n+1/2}(\varphi^{(1)}_{n+1} - \varphi^{(1)}_n, \varphi^{(2)}_{n+1} - \varphi^{(2)}_n) &= \int_{\Gamma_C^{(1)}} \Lambda_{n+1/2}\, \hat{\nu}_{n+1/2} \cdot \delta\varphi_n \\ &= \int_{\Gamma_C^{(1)}} \Lambda_{n+1/2}\, \delta g_n \\ &= \frac{1}{2}\int_{\Gamma_C^{(1)}} \lambda_{n+1} g_{n+1} - \lambda_n g_n, \end{aligned}$$

hence the proof. □

Remark 9 *In the above formulation, the angular momentum is not exactly conserved:*

$$\begin{aligned} &\Delta t\; G_{n+1/2}(a \times \varphi^{(1)}_{n+/2}, a \times \varphi^{(2)}_{n+/2}) \\ &= a \cdot \Delta t \int_{\Gamma_C} \Lambda_{n+1/2}\, \hat{\nu}_{n+1/2} \times (\varphi^{(1)}_{n+1/2} - \varphi^{(2)}_{n+1/2}) \\ &= a \cdot \Delta t \int_{\Gamma_C} \Lambda_{n+1/2}\, g_{n+1/2}\, \hat{\nu}_{n+1/2} \times \nu_{n+1/2} \\ &= a \cdot \Delta t \int_{\Gamma_C} \Lambda_{n+1/2}\, g_{n+1/2}\, \hat{\nu}_{n+1/2} \times (\nu_{n+1/2} - \hat{\nu}_{n+1/2}) \\ &= O(\eta \Delta t^3). \end{aligned}$$

A small error is therefore introduced by the scheme due to the unexact colinearity of $\nu_{n+1/2}$ and $\hat{\nu}_{n+1/2}$.

Remark 10 *When dealing with an exact non-penetration condition (rather than penalized), the following discrete persistency condition should be enforced:*

$$\Lambda_{n+1/2}\frac{g_{n+1}-g_n}{\Delta t_n}=0.$$

Remark 11 *A more naive energy conserving formulation is given by:*

$$G_{n+1/2}(v^{(1)},v^{(2)})=\int_{\Gamma_C^{(1)}} N_{n+1/2}\cdot\left[v^{(1)}(x)-v^{(2)}(\overline{y}_{n+1/2}(x))\right], \qquad (46)$$

in which:

$$N_{n+1/2}=\lambda_{n+1/2}\nu_{n+1/2}-\left[\frac{\lambda_{n+1}g_{n+1}-\lambda_n g_n}{2}-\lambda_{n+1/2}\nu_{n+1/2}\cdot\delta\varphi_n\right]\frac{\delta\varphi_n}{\delta\varphi_n\cdot\delta\varphi_n},$$

with the above notation. But this choice does not properly preserve the orientation of the reaction force as shown in the case of unilateral frictionless contact against a plane wall.

5.1.4 Unilateral frictionless contact against a plane wall

We analyze here the case of unilateral frictionless contact against a plane wall. Then, we assume that the infinite half space $\Omega^{(2)}=\mathbb{R}^2\times\mathbb{R}_+$ is fixed and perfectly rigid, and that the deformable body $\Omega^{(1)}$ is submitted to a unilateral frictionless contact against the boundary $\Gamma_C^{(2)}=\mathbb{R}^2\times\{0\}$ of $\Omega^{(2)}$. This assumption imposes that the displacement fields $\varphi^{(2)}=id$ and its variations $v^{(2)}$ vanish. Moreover, the outward normal unit vector ν is constant over $\Gamma_C^{(2)}$. Then, by using the above definitions, we get:

$$\begin{cases}\overline{y}_n(x)=\varphi_n(x)-(\varphi_n(x)\cdot\nu)\nu,\\ g_n(x)=-\varphi_n^{(1)}(x)\cdot\nu,\\ \delta\varphi_n(x)=\varphi_{n+1}^{(1)}(x)-\varphi_n^{(1)}(x)\end{cases}$$

and deduce that $\hat{\nu}_{n+1/2}(x)=-\nu$, so that:

$$G_{n+1/2}(v^{(1)},0)=-\int_{\Gamma_C^{(1)}}\Lambda_{n+1/2}\;\nu\cdot v^{(1)},\forall v^{(1)}\in\mathcal{U}_0(\Omega^{(1)})$$

with $\Lambda_{n+1/2}$ as defined in (43). Observe here that the contact force is normal to the wall as expected, but it would not be the case for the apparently simpler formulation (46). Indeed, the latter induces a non-physical variation of the contact force direction to achieve energy conservation, while (41) only plays on the intensity of the contact force. Moreover, the choice (41) turns out to be numerically more efficient with a nonlinear solution easier to catch.

5.2.1 A two-branch model

The multibranch viscoelastic incompressible model presented in [37,29] introduces in addition to the displacements and hydrostatic pressures fields φ,p of the hyperelastic framework, volume-preserving symmetric positive second order tensors A of internal variables, which formally represent the inverse of the right Cauchy-Green strain tensor inside each viscous branch. The hyperelastic stored energy function $\mathcal{W}(C)$ becomes $\tilde{\mathcal{W}}(C, A)$ with typically, in the case of a single viscous branch:

$$\tilde{\mathcal{W}}(C, A) = \mathcal{W}(C) + \mathcal{W}_e(A^{1/2} \cdot C \cdot A^{1/2}).$$

Here $\mathcal{W}_e$ is the stored elastic energy in the viscous branch of the material. The time evolution of the internal variable A is governed by an energy dissipating time evolution equation such as

$$\begin{cases} \nu\, \partial_t(A(t)^{-1}) = \dfrac{\partial \tilde{\mathcal{W}}}{\partial A} - q(t)\, cof\, A(t), \\ \det A(t) - 1 - \eta_v q(t) = 0. \end{cases} \tag{47}$$

Proposition 8 *[37,31] The viscoelastic variational problem (4),(47) conserves linear and angular momenta, and the time evolution of its energy is given by:*

$$\mathcal{E}(t) - \mathcal{E}(0) = \int_0^t \left(\int_\Omega f(s) \cdot \dot{\varphi}(s) + \int_{\Gamma_N} g(s) \cdot \dot{\varphi}(s) - \int_\Omega \nu D(s) : D(s) \right) ds,$$

where the viscous deformation rate tensor and the total energy are respectively given by:

$$D(t) = A(t)^{-1/2} \cdot \dot{A}(t) \cdot A(t)^{-1/2},$$

$$\mathcal{E}(t) = \int_\Omega \rho \dot{\varphi}(t)^2 + \int_\Omega \tilde{\mathcal{W}}(C(t), A(t)) + \frac{\epsilon}{2} \int_\Omega p(t)^2 + \frac{\eta_v}{2} \int_\Omega q(t)^2.$$

$$
\begin{aligned}
&\mathcal{T}_{n+1/2}(\hat{\varphi},\hat{A}) = \\
&\int_\Omega 2\ F_{n+1/2}\cdot\frac{\partial\tilde{\mathcal{W}}}{\partial C}(C_{n+1/2},A_{n+1/2}) : \nabla\hat{\varphi} + \frac{\partial\tilde{\mathcal{W}}}{\partial A}(C_{n+1/2},A_{n+1/2}) : \hat{A} \\
&-2\ p_{n+1/2}\ F_{n+1/2}\cdot\frac{\partial \det C^{1/2}}{\partial C}(C_{n+1/2}) : \nabla\hat{\varphi} + q_{n+1/2}\ \ cof\ A_{n+1/2} : \hat{A} \\
&+\left[\tilde{\mathcal{W}}(C_{n+1},A_{n+1}) - \tilde{\mathcal{W}}(C_n,A_n)\right]\frac{2(\delta C_n : F^t_{n+1/2}\cdot\nabla\hat{\varphi}) + (\delta A_n : \hat{A})}{(\delta C_n : \delta C_n) + (\delta A_n : \delta A_n)} \\
&-\left[\frac{\partial\tilde{\mathcal{W}}}{\partial C}(C_{n+1/2},A_{n+1/2}) : \delta C_n + \frac{\partial\tilde{\mathcal{W}}}{\partial A}(C_{n+1/2},A_{n+1/2}) : \delta A_n\right]\times \\
&\qquad\qquad\times\frac{2(\delta C_n : F^t_{n+1/2}\cdot\nabla\hat{\varphi}) + (\delta A_n : \hat{A})}{(\delta C_n : \delta C_n) + (\delta A_n : \delta A_n)} \\
&-2\ p_{n+1/2}\left[\det F_{n+1} - \det F_n - \frac{\partial \det C^{1/2}}{\partial C}(C_{n+1/2}) : \delta C_n\right]\frac{\delta C_n : F^t_{n+1/2}\cdot\nabla\hat{\varphi}}{\delta C_n : \delta C_n} \\
&+q_{n+1/2}\left[\det A_{n+1} - \det A_n - cof\ A_{n+1/2} : \delta A_n\right]\frac{\delta A_n : \hat{A}}{\delta A_n : \delta A_n}.
\end{aligned}
\tag{49}
$$

Fig. 2. Expression of $\mathcal{T}_{n+1/2}(\hat{\varphi},\hat{A})$ achieving an exact discrete balance in (48).

5.2.2 Time integration scheme

We extend the energy-conserving scheme to this situation, and propose a time integration procedure for the viscoelastic problem (4),(47) as follows:

$$
\begin{cases}
\displaystyle\int_\Omega \rho\frac{\dot{\varphi}_{n+1}-\dot{\varphi}_n}{\Delta t_n}\cdot\hat{\varphi} + \int_\Omega \nu\ \left(\left(\frac{A_n+A_{n+1}}{2}\right)^{-1}\cdot\frac{A_{n+1}-A_n}{\Delta t_n}\cdot\left(\frac{A_n+A_{n+1}}{2}\right)^{-1}\right) : \hat{A} \\
\displaystyle +\mathcal{T}_{n+1/2}(\hat{\varphi},\hat{A}) = \int_\Omega \frac{f_n+f_{n+1}}{2}\cdot\hat{\varphi} + \int_{\Gamma_N}\frac{g_n+g_{n+1}}{2}\cdot\hat{\varphi}, \qquad \forall(\hat{\varphi},\hat{A})\in\mathcal{U}_0\times\mathcal{A}, \\
\displaystyle\frac{\varphi_{n+1}-\varphi_n}{\Delta t_n} = \frac{\dot{\varphi}_n+\dot{\varphi}_{n+1}}{2} \text{ trapezoidal rule on acceleration} \\
\displaystyle\int_\Omega(\det\nabla\varphi_{n+1} - 1 + \epsilon p_{n+1})\hat{p} = 0, \qquad \forall\hat{p}\in\mathcal{P}, \\
\displaystyle\int_\Omega(\det A_{n+1} - 1 - \eta_v q_{n+1})\hat{q} = 0, \qquad \forall\hat{q}\in\mathcal{Q},
\end{cases}
\tag{48}
$$

where the stress term $\mathcal{T}_{n+1/2}(\hat{\varphi},\hat{A})$ is given for all $(\hat{\varphi},\hat{A})\in\mathcal{U}_0\times\mathcal{A}$ by the energy-conserving expression detailed in figure 2. We have adopted the obvious notation $\square_{n+1/2} = \dfrac{\square_n+\square_{n+1}}{2}$ and $\delta\square_n = \square_{n+1}-\square_n$. The expression of $\mathcal{T}_{n+1/2}(\hat{\varphi},\hat{A})$ given by (49) is in fact a second order accurate approximation in

time of

$$\int_\Omega 2F \cdot \frac{\partial \mathcal{W}}{\partial C}(C,A) : \nabla \hat{\varphi} + \int_\Omega \frac{\partial \mathcal{W}}{\partial A}(C,A) : \hat{A},$$

at time $t_{n+1/2}$, and therefore the time integration scheme (48) is second order accurate. In the definition (49) of $\mathcal{T}_{n+1/2}(\hat{\varphi}, \hat{A})$, the four last lines correspond to energy correction terms enabling energy conservation in the way proposed by O. Gonzalez [3].

Proposition 9 *The discrete solution given by (48) conserves linear and angular momenta and the discrete time evolution of its energy is given by:*

$$\mathcal{E}_{n+1} - \mathcal{E}_n = \int_\Omega \frac{f_n + f_{n+1}}{2} \cdot \frac{\dot{\varphi}_n + \dot{\varphi}_{n+1}}{2}$$

$$+ \int_{\Gamma_N} \frac{g_n + g_{n+1}}{2} \cdot \frac{\dot{\varphi}_n + \dot{\varphi}_{n+1}}{2} - \int_\Omega \nu \; D_{n+1/2} : D_{n+1/2},$$

with the discrete deformation rate tensor and the discrete total energy given by

$$D_{n+1/2} = \left(\frac{A_n + A_{n+1}}{2}\right)^{-1/2} \cdot \frac{A_{n+1} - A_n}{\Delta t_n} \cdot \left(\frac{A_n + A_{n+1}}{2}\right)^{-1/2},$$

$$\mathcal{E}_n = \frac{1}{2}\int_\Omega \rho \dot{\varphi}_n^2 + \int_\Omega \tilde{\mathcal{W}}(C_n, A_n) + \frac{\epsilon}{2}\int_\Omega p_n^2 + \frac{\eta_v}{2}\int_\Omega q_n^2.$$

Proof : Energy conservation is obtained by taking $\hat{\varphi} = \dfrac{\varphi_{n+1} - \varphi_n}{\Delta t_n}$ and $\hat{A} = \dfrac{A_{n+1} - A_n}{\Delta t_n}$ in (48). By construction of $\mathcal{T}_{n+1/2}$, we get:

$$\mathcal{T}_{n+1/2}\left(\frac{\varphi_{n+1} - \varphi_n}{\Delta t_n}, \frac{A_{n+1} - A_n}{\Delta t_n}\right) = \frac{1}{\Delta t_n}\int_\Omega \tilde{W}(C_{n+1}, A_{n+1}) - \tilde{W}(C_n, A_n)$$

$$-\frac{1}{\Delta t_n}\int_\Omega p_{n+1/2}\left(\det C_{n+1}^{1/2} - \det C_n^{1/2}\right) + \frac{1}{\Delta t_n}\int_\Omega q_{n+1/2}\left(\det A_{n+1} - \det A_n\right),$$

which, plugged into (48) and used with the quasi-incompressibility constraints yields

$$\int_\Omega \rho \frac{\dot{\varphi}_{n+1} - \dot{\varphi}_n}{\Delta t_n} \cdot \frac{\varphi_{n+1} - \varphi_n}{\Delta t_n} + \int_\Omega \nu D_{n+1/2} : D_{n+1/2}$$

$$+\frac{1}{\Delta t_n}\int_\Omega \tilde{W}(C_{n+1}, A_{n+1}) - \tilde{W}(C_n, A_n) + \frac{\epsilon}{2\Delta t_n}\int_\Omega (p_{n+1}^2 - p_n^2) + \frac{\eta_v}{2\Delta t_n}\int_\Omega (q_{n+1}^2 - q_n^2)$$

$$= \int_\Omega \frac{f_n + f_{n+1}}{2} \cdot \frac{\varphi_{n+1} - \varphi_n}{\Delta t_n} + \int_{\Gamma_N} \frac{g_n + g_{n+1}}{2} \cdot \frac{\varphi_{n+1} - \varphi_n}{\Delta t_n}.$$

The discrete energy conservation result is then straightforward by using Newmark's trapezoidal rule: $\frac{\varphi_{n+1} - \varphi_n}{\Delta t_n} = \frac{\dot{\varphi}_n + \dot{\varphi}_{n+1}}{2}$. □

5.2.3 Simplified energy

In many engineering applications, viscoelasticity is often a perturbation of the underlying hyperelastic model. We can then use very simple laws in the viscous branch. We choose herein a stored elastic energy in the viscous branch which only depends on the first invariant of the elastic tensor $C_e = A^{1/2} \cdot C \cdot A^{1/2}$ in the branch:

$$W_e(C_e) = \frac{G}{2} \ (tr\, C_e - 3)^2 = \frac{G}{2} \ (tr(C \cdot A) - 3)^2 \,.$$

The stress correction of section 5.2 then reduces to:

$$\mathcal{T}_{n+1/2}(\hat{\varphi}, \hat{A}) = \int_\Omega 2F_{n+1/2} \cdot \left(\Sigma_{n+1/2} + \mathcal{S}_{n+1/2} \ A_{n+1/2}\right) : \nabla\hat{\varphi}$$

$$+ \int_\Omega \mathcal{S}_{n+1/2} \ C_{n+1/2} : \hat{A},$$

with

$$\mathcal{S}_{n+1/2} = G \ \left[tr\left(\frac{C_n \cdot A_n + C_{n+1} \cdot A_{n+1}}{2}\right) - 3\right],$$

and $\Sigma_{n+1/2}$ the "conservative" Gonzalez algorithmic Piola-Kirchhoff second stress tensor. A straightforward computation then gives:

$$\mathcal{T}_{n+1/2}(\varphi_{n+1} - \varphi_n, A_{n+1} - A_n) = \tilde{W}(C_{n+1}, A_{n+1}) - \tilde{W}(C_n, A_n),$$

with:

$$\tilde{W}(C_n, A_n) = \hat{W}(\nabla\varphi_n) + \frac{G}{2} \ (tr(C_n \cdot A_n) - 3)^2 \,.$$

At each time step t_n, A_n is taken piecewise constant on each element of the mesh.

Remark 12 *The solution of the fully coupled visco-elastic problem (48) at time t_{n+1} can be obained by the following staggered algorithm:*

(1) initialize $A^{(0)}_{n+1} = A_n$, $k = 0$,
(2) solve the hyperelastic part in (48) -i.e with $\hat{A} = 0$- imposing the value $A^{(k)}_{n+1}$, to get $\varphi^{(k)}_{n+1}$,
(3) solve the evolution of the internal variable in (48) -i.e with $\hat{\varphi} = 0$- imposing the value $C^{(k)}_{n+1}$, to get $A^{(k+1)}_{n+1}$,
(4) go to step 2 with $k \leftarrow k + 1$, until convergence of $A^{(k)}_{n+1}$.

6 Numerical validation

As the time step goes to zero, the aforementioned second order schemes show similar results (they share an asymptotic second order accuracy). Rather than

illustrating convergence features, the purpose of the following examples is to illustrate their differences in terms of conservation of the main invariants or stability when using *physically relevant time steps*.

6.1 Cantilever beam

Let us consider here the time evolution of an homogeneous compressible cantilever beam oscillating under the action of a vertical static load F applied at its tip. The adopted constitutive law is:

$$\mathcal{W}(C) = a\, tr\, C + b\, tr\, cof\, C + c \det C - d \log \det C + e.$$

Data is detailed on figure 3 together with the static equilibrium configuration of the beam. The selected time discretization uses twenty time step per "period" ($\Delta t = 0.05$ s), and a special attention is paid to the evolution of the following discrete energy:

$$\mathcal{H}_n := \mathcal{E}_n - \int_{tip} F \cdot \varphi_n = \frac{1}{2}\int_\Omega \rho \dot{\varphi}_n^2 + \int_\Omega \mathcal{W}(C_n) - \int_{tip} F \cdot \varphi_n.$$

The nonlinear problems occuring at each time step are solved by the Newton-Raphson algorithm, the L^2 norm of the residual at convergence being less than 1.E-9.

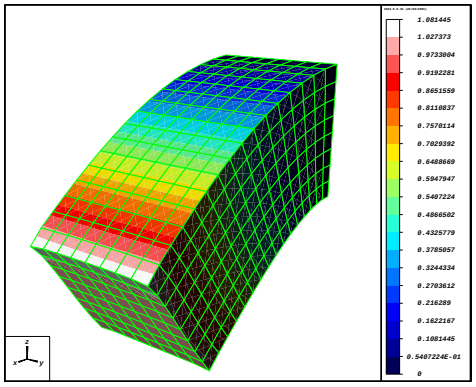

- length = 2m,
- width = 1m,
- density ρ = 1200 kg/m3,
- c_1 = 0.2 MPa,
- c_2 = 2 kPa,
- c_3 = 0.4 MPa,
- $d = c_1 + 2c_2 + c_3$,
- $e = -3a - 3b - c$,
- F= 24 kN.

Fig. 3. Static equilibrium of the beam under loading and constitutive data.

As expected, and in agreement with previous observations (see for instance [4,20,21]), midpoint and trapezoidal strategies encounter a severe energy blow up (figure 4). Observe that such a lack of control occurs in spite of the symplecticity of the midpoint strategy as reported in [11]. HHT scheme is less predictable because its stability depends on the value of the regularization coefficient α, on the stiffness of the model and the time step. Accretive or dissipative behaviors can be observed indifferently. The fact that a correct behavior is obtained here around the value $\alpha = 0.05$ which is recommended in [1,34,7] corresponds to a pure coincidence in the choice of the parameters

of the model. At the opposite, energy blow up is observed for $\alpha = 0.005$. The critical value of α beyond which the HHT scheme becomes dissipative is really case-dependent. There is in fact no evidence that one can always obtain a dissipative HHT scheme for sufficiently large values of α.

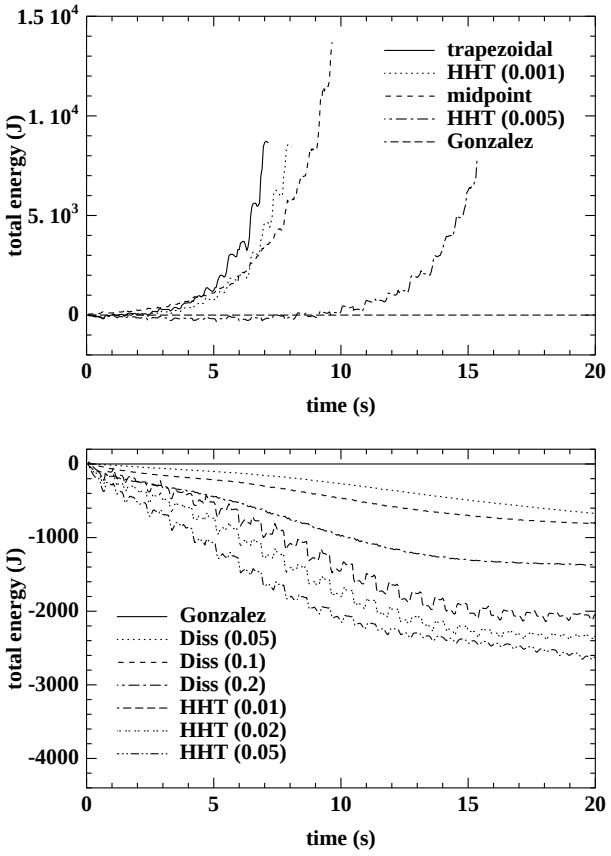

Fig. 4. Evolution of the discrete energy $\mathcal{H}_n$ for the different schemes (for reader's convenience, the schemes are listed in the order of decreasing energies). The values of α appear between parentheses in the legend. For HHT, $\alpha = 0.01$, 0.02, 0.05 and for our dissipative scheme $\alpha = 0.05$, 0.1, 0.2.

On the other hand, Gonzalez energy-conserving scheme [3] achieves here a perfect control of stability (see figure 4). Nevertheless, as observed at the tip of the beam, velocities present high frequency components (figure 5). The dissipation strategy proposed in this paper to damp out energy at highest frequencies provides a clear regularization of the velocities (figure 5 with $\alpha = 0.2$). The associated energy evolution appears on figure 4 for different values of α (specified in the legend). The fundamental difference with the standard HHT scheme is a perfect conservation of momenta, and an unconditional dissipative behavior for $\alpha > 0$.

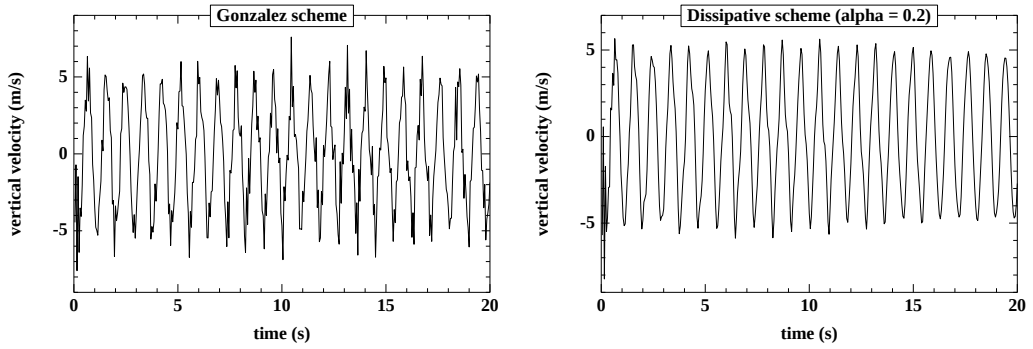

Fig. 5. Time evolution of the velocity at the tip of the beam for Gonzalez conservative scheme and our dissipative variant ($\alpha = 0.2$).

6.2 Ball impact at low velocity

Let us consider now a hollow ball with a small cylindrical hole, made of a compressible material, with computational and physical data given in figure 6. The nonlinear problems occuring at each time step are solved by the Newton-Raphson algorithm, and the L^2 norm of the residual at convergence is less than 1.E-6.

A snapshot of the impact simulation against a plane wall is shown on figure 7, and as illustrated on figure 8, the evolution of the discrete energy in the ball is very sensitive to the time integration strategy.

radius	0.1 m	η	1.E-4
density	1200 kg/m^3	Δt	0.002 s
Young's modulus	0.2 M Pa	T	1.0 s
Poisson's ratio	0.33	# nodes in the mesh	11 160
initial velocity	0.4 m/s		

Fig. 6. Data for ball impact; Saint-Venant/Kirchhoff material.

In particular, the discrete energy explodes when using a midpoint scheme (or a trapezoidal scheme). The conservative Gonzalez scheme enriched with our energy conserving impact formulation keeps its promise. The relative loss of energy through the impact is 1.8 E-4, and only depends on the required accuracy in Newton's algorithm. The interest of our energy dissipative formulation is also confirmed, showing here the control of the energy in the ball.

To complete this discussion, let us mention that when considering industrial

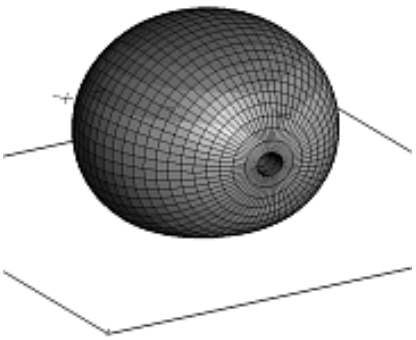

Fig. 7. Snapshot of the impact simulation.

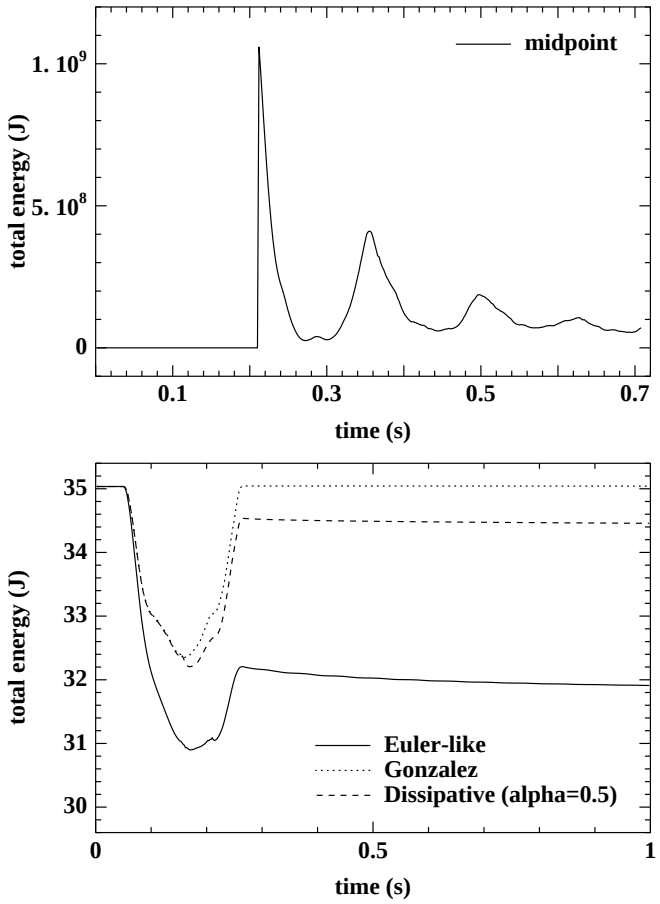

Fig. 8. Evolution of the total energy of the ball through impact for midpoint, Euler-Newmark, energy conserving, and dissipating ($\alpha = 0.5$) schemes.

simulation for non-smooth dynamics, first order implicit schemes are sometimes preferred for their robustness, especially in coupled systems [38,39]. Let us introduce the following time integration approach obtained by a trapezoidal integration of the inertial term, and an implicit Euler strategy for the stress

part:

$$\begin{cases} \displaystyle\int_\Omega \rho \frac{\dot\varphi_{n+1} - \dot\varphi_n}{\Delta t_n} \cdot v + \int_\Omega \frac{\partial \hat{\mathcal{W}}}{\partial F}(\nabla \varphi_{n+1}) : \nabla v = \int_\Omega \frac{f_n + f_{n+1}}{2} \cdot v, \quad \forall v \in \mathcal{U}_0, \\ \displaystyle\frac{\varphi_{n+1} - \varphi_n}{\Delta t_n} = \frac{\dot\varphi_n - \dot\varphi_{n+1}}{2}. \end{cases} \tag{50}$$

It is first order accurate, and written here in the compressible framework. Kinematical constraints will be naturally satisfied by the displacements field φ_{n+1} at time t_{n+1}. It is a Euler-like degraded first order version of the trapezoidal second order time integration scheme. It can be readily checked with the analysis of section 4, that the Euler-Newmark scheme (50) is energy dissipating whenever the stored energy $\hat{\mathcal{W}}(F)$ is locally convex. The ball impact simulation performed with this scheme proves to achieve global energy dissipation, with a 9 % relative loss of energy through the impact. To illustrate the better accuracy of our second order energy conserving/dissipating schemes, figure 9 shows the evolution of elastic energy after impact.

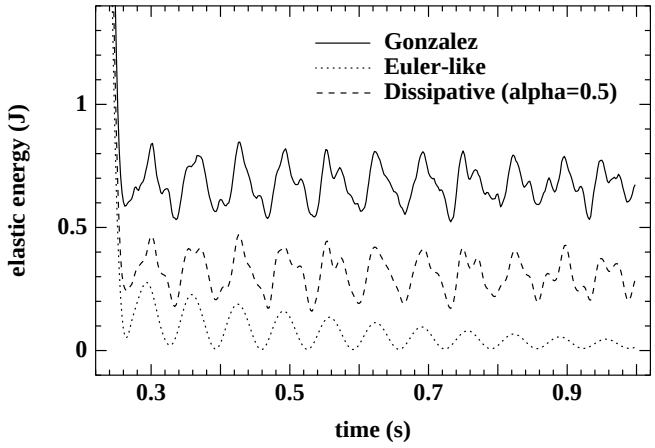

Fig. 9. Evolution of elastic energy after impact for first order Euler-Newmark scheme, and second order energy conserving and dissipating ($\alpha = 0.5$) schemes.

Finally, we use the present example to illustrate the well-known sensitivity of contact pressures to the penalization coefficient η. Indeed, it is shown on figure 10 that when η is divided by 10, oscillations on the contact force appear. Such a phenomenon is discussed in [27] and in associated references. It is due to a lack of strong convergence of the solution when the penalty term goes to zero.

6.3 Low-velocity impact of an incompressible viscoelastic body

A first illustration on the model beam problem of section 6.1 (with the same parameters) indicates that the presence of a realistic dissipative viscoelastic branch (with $G = 0.2\, c_1 = 40$ kPa) does not prevent the energy from

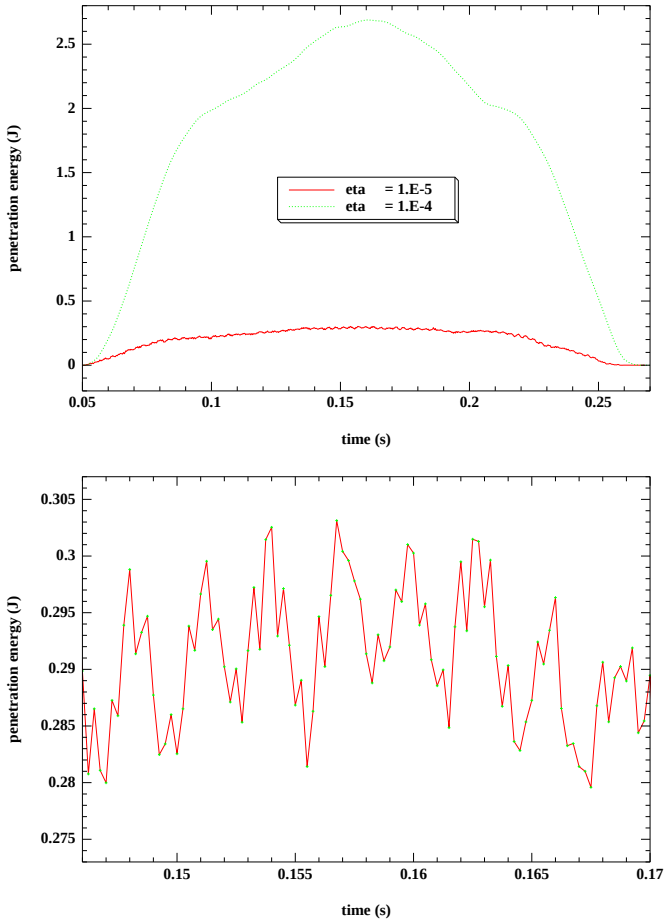

Fig. 10. Evolution of penetration energy during ball impact for η = 1.E-4 and η = 1.E-5 (top), and zoom on the oscillations for η = 1.E-5 (bottom).

blowing when using the midpoint rule for both the hyperelastic and viscoelastic branches (figure 11). When using the proposed conservative scheme with trapezoidal integration of accelerations ($\alpha = 0$), it is shown on the other hand that energy dissipation is in fact much greater than the energy dissipated by the regularization of section 4.2. (compare figures 4 and 12). In fact, as soon as the hyperelastic branch is integrated by a conservative scheme, using either a midpoint or a conservative integration of the viscoelastic branch yields the same results in terms of energy dissipation. Nevertheless, a difference in the values obtained for the viscoelastic variable A can be observed (figure 13). In practice, we have also observed that the use of the proposed conservative integration for the viscoelastic branch entails no computational overcost, and guarantees an exact energy balance at convergence.

Next, we study the impact of a viscoelastic ball (figure 15) made of an incompressible material, with data given on figure 14. For this problem, the use of a robust energy-conserving algorithm makes it possible to use reasonnably large time steps (Δt= 2.E-4 s for which contact oscillations are not accurately

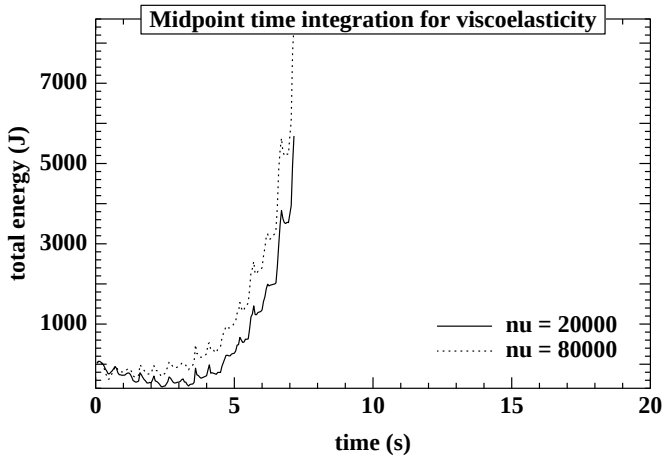

Fig. 11. Evolution of discrete total energy for the viscoelastic beam. The integration of both hyperelastic and viscoelastic branches uses a midpoint scheme. Different values of $\nu = 20000$, 80000 are represented.

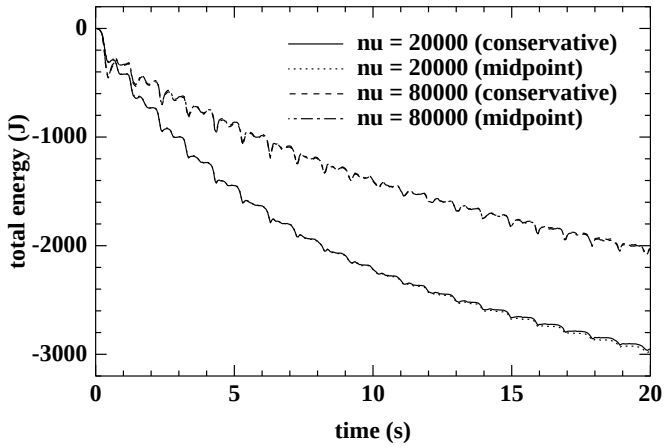

Fig. 12. Evolution of discrete total energy for the viscoelastic beam. The integration of the hyperelastic branch uses a conservative scheme. Different values of ν are represented. The viscoelastic branch is integrated either by the midpoint rule or our conservative approach, which is indicated between parentheses in the legend. For the same value of ν, the two curves adopting different integration strategies for the viscous branch show almost identical results.

forecast). Contact remains integrated while achieving a perfect conservation of the main invariants. Additionally, the nonlinear problems occuring at each time step are solved by the Newton-Raphson algorithm, ensuring that the L^2 norm of the residual is less than 1.E-5. Here, in spite of this large time step, the midpoint rule remains stable for the elastic case unlike the previous section (figure 17), although the slope in the energy curve after contact seems to indicate a long-term instability. Adding a viscoelastic behavior ($\nu = 200$, $G = 50$ kPa) does not add dissipation in the energy curve for the midpoint rule, the energy growth being in fact worse than for the hyperelastic case (figure 17). In contrast, our conservative scheme involving a proper formulation of

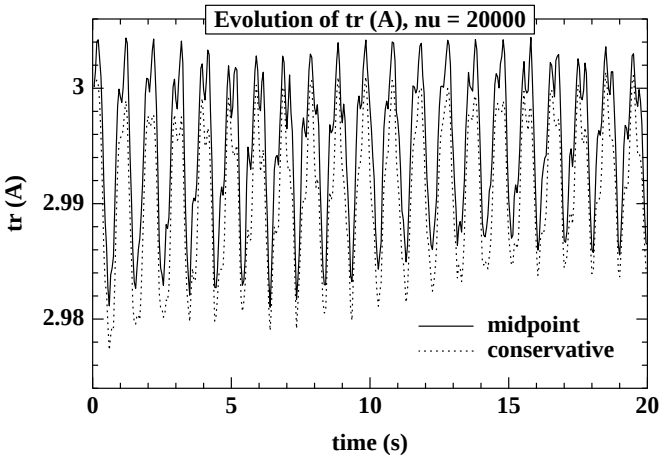

Fig. 13. Evolution of trA for an element in the middle of the beam when the integration of the hyperelastic branch uses a conservative scheme. The viscoelastic branch is integrated either by the midpoint rule or by our conservative approach.

contact and viscoelasticity gives accurate consistent results on the energy.

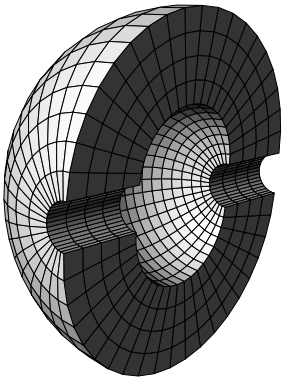

$\rho = 1500$ kg/m3
Mooney-Rivlin material:
$c_1 = 0.2$ MPa
$c_2 = 2000$ Pa
$\epsilon^{-1} = 2.\text{E}8$
$\eta^{-1} = 1.\text{E}18$
Velocity = 7 m/s
3040 hexaedra mesh

Fig. 14. Section of the ball and main characteristics

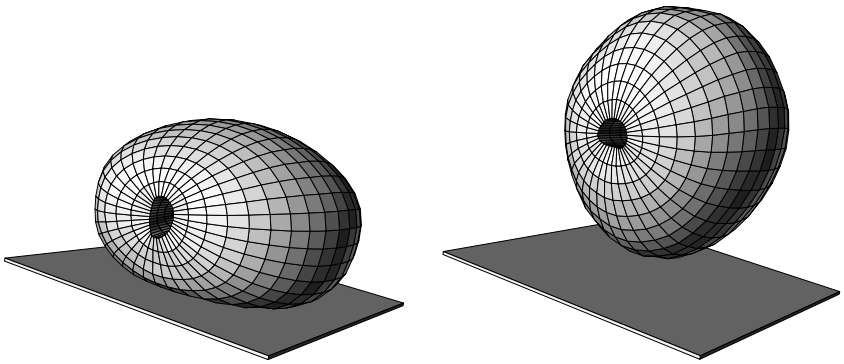

Fig. 15. Snapshots of the ball during and after impact.

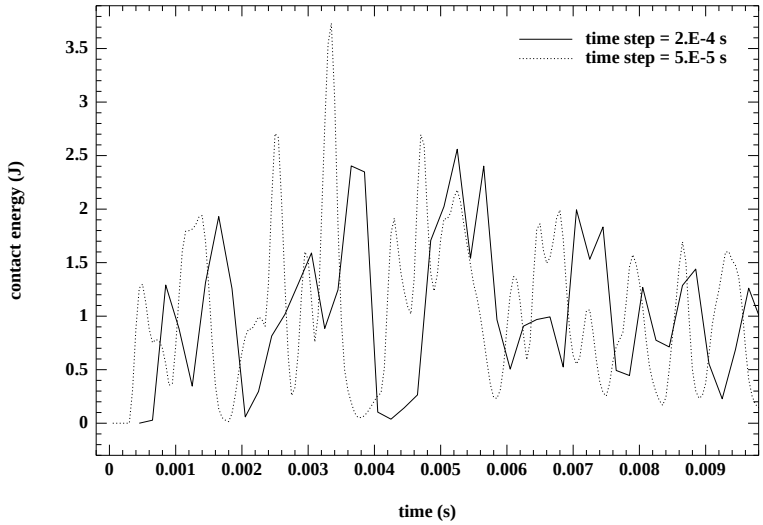

Fig. 16. Comparison in terms of penetration energy of the fine integration of contact (time step = 5.E-5 s) with a coarse one (time step = 2.E-4 s) describing the evolution of contact without accuracy.

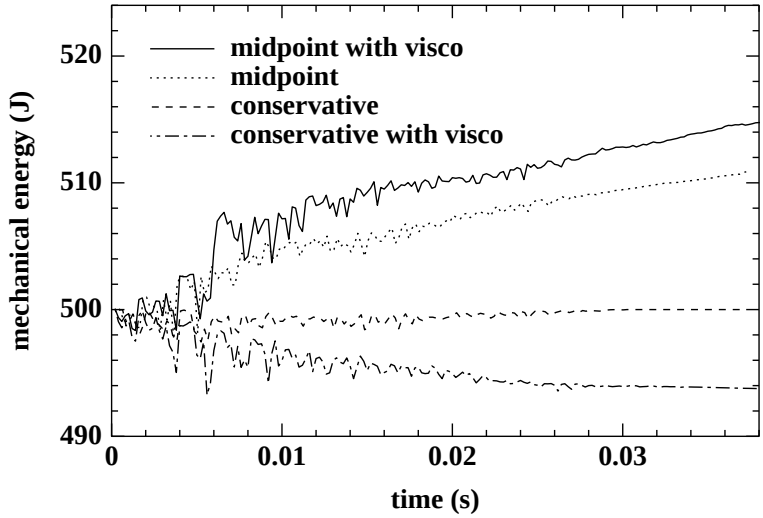

Fig. 17. Evolution of the mechanical energy in the ball for the dynamics integrated by midpoint and conservative schemes; hyperelastic and viscoelastic behaviors.

7 Conclusion

In this paper, we have proposed a detailed analysis of the non-conservative properties of midpoint, trapezoidal and HHT time integration schemes in incompressible nonlinear elasticity, and compared them to the theoretical performances of an energy conserving scheme. Moreover, we have used the analysis done for the HHT method to propose a new energy-dissipative momenta-conserving discrete integrator in the nonlinear framework, involving a regularized energy taking acceleration effects into account. Finally, by generaliz-

ing Gonzalez energy correction method [3], we have proposed a conservative strategy for penalized frictionless impact problems enforcing the usual Kuhn-Tucker conditions at entire time steps. An extension to viscoelasticity is also proposed, and the analysis of these techniques is illustrated with numerical simulations.

Energy conservation is even more crucial when considering the dynamics of coupled problems, such as aeroelasticity [40] or magneto-hydro-dynamics [39]. We believe that the conservative philosophy developed in this paper can be successfully extended to complex coupled problems. In particular, we have shown in [41,42] that the energy-conserving approach presented herein could be extended to a fluid-structure interaction framework.

Acknowledgement

P.H. would like to gratefully acknowledge the support of Michelin Tire Company during the completion of this work at the Center of Applied Mathematics (CMAP), Ecole Polytechnique. Moreover, we would like to express our gratitude to Professor François Jouve for providing his finite element code, developed at CMAP, Ecole Polytechnique, in which the presented ideas have been implemented. The fruitful comments and suggestions of the anonymous referees are also sincerely acknowledged.

References

[1] H. Hilber, T. Hughes, R. Taylor, Improved numerical dissipation for time integration algorithms in structural dynamics, Earthquake Engin. and Struct. Dynamics 5 (1977) 283–292.

[2] J. Simo, N. Tarnow, The discrete energy-momentum method. conserving algorithms for non linear elastodynamics, Z angew Math Phys 43 (1992) 757–792.

[3] O. Gonzalez, Exact energy and momentum conserving algorithms for general models in nonlinear elasticity, Comput. Methods Appl. Mech. Engrg. 190 (13-14) (2000) 1763–1783.

[4] T. Laursen, X. Meng, A new solution procedure for application of energy-conserving algorithms to general constitutive models in nonlinear elastodynamics, Computer Methods in Appl. Mech. and Eng. 190 (2001) 6309–6322.

[5] C. Sansour, P. Wriggers, J. Sansour, On the design of energy-momentum integration schemes for arbitrary continuum formulations. applications to classical and chaotic motion of shells, International Journal for Numerical Methods in Engineering 60 (2004) 2419–2440.

[6] K.-J. Bathe, Finite element procedures in engineering analysis, Prentice-Hall, 1982.

[7] M. Crisfield, Nonlinear finite element analysis of solids and structures, Vol. 2: Advanced topics, Wiley, 1997.

[8] M. Géradin, D. Rixen, Théorie des vibrations: application la dynamique des structures, Masson, 1993.

[9] E. Hairer, C. Lubich, G. Wanner, Geometric Numerical Integration, Springer-Verlag, 2002.

[10] J. Sanz-Serna, M. Calvo, Numerical Hamiltonian Problems, Chapman & Hall, 1994.

[11] J. Simo, O. Gonzalez, Assessment of energy-momentum and symplectic schemes for stiff dynamical systems, in: American Society of Mechanical Engineers, ASME Winter Annual Meeting, New Orleans, Louisiana, 1993.

[12] C. Kane, J. Marsden, M. Ortiz, M. West, Variational integrators and the Newmark algorithm for conservative and dissipative mechanical systems, International Journal for Numerical Methods in Engineering 49 (2000) 1295–1325.

[13] J. Marsden, M. West, Acta Numerica, Cambridge University Press, 2001, Ch. Discrete mechanics and variational integrators, pp. 357–514.

[14] A. Lew, J.-E. Marsden, M. Ortiz, M. West, Asynchronous variational integrators, Arch. Ration. Mech. Anal.

[15] S. Müller, M. Ortiz, On the Γ-convergence of discrete dynamics and variational integrators, J. Nonlinear Sci. 14 (2004) 276–296.

[16] E. Naug, O. Nguyen, A. D. Rouvray, An improved energy conserving implicit time integration algorithm for nonlinear dynamic structural analysis, in: Proceedings of the Fourth Conference on Structural Mechanics in Reactor Technology, San Francisco, 1977.

[17] T. Hughes, W. Liu, Caughy, Transient finite element formulations that preserve energy, Journal of Applied Mathematics 45 (1978) 366–370.

[18] H. Munthe-Kass, High order runge-kutta methods on manifolds, Applied Numerical Mathematics 29 (1999) 115–127.

[19] P. Betsch, P. Steinmann, Conservation properties of a time FE method - ii: time-stepping schemes for non-linear elastodynamics, International Journal for Numerical Methods in Engineering 50 (2001) 1931–1955.

[20] F. Armero, I. Romero, On the formulation of high-frequency dissipative time-stepping algorithms for nonlinear dynamics. part i: low-order methods for two model problems and nonlinear elastodynamics, Comput. Methods Appl. Mech. Engrg. 190 (20-21) (2001) 2603–2649.

[21] F. Armero, I. Romero, On the formulation of high-frequency dissipative time-stepping algorithms for nonlinear dynamics. part ii: second-order methods, Comput. Methods Appl. Mech. Engrg. 190 (51-52) (2001) 6783–6824.

[22] M. Borri, C. Botasso, L. Trainelli, Integration of elastic multibody systems by invariant conserving/dissipating algorithms. part i: Formulation, Comput. Methods Appl. Mech. Engrg. 190 (2001) 3669–3699.

[23] M. Borri, C. Botasso, L. Trainelli, Integration of elastic multibody systems by invariant conserving/dissipating algorithms. part ii: Numerical schemes and applications, Comput. Methods Appl. Mech. Engrg. 190 (2001) 3701–3733.

[24] M. Borri, C. Botasso, L. Trainelli, Robust integration schemes for flexible multibody systems, Comput. Methods Appl. Mech. Engrg. 192 (2003) 395–420.

[25] Q. Bui, Energy dissipative time finite elements for classical mechanics, Comput. Methods Appl. Mech. Engrg. 192 (2003) 2925–2947.

[26] T. Laursen, V. Chawla, Design of energy conserving algorithms for frictionless dynamic contact problems, International Journal for Numerical Methods in Engineering 40 (1997) 863–886.

[27] F. Armero, E. Petöcz, Formulation and analysis of conserving algorithms for frictionless dynamic contact/impact problems, Comput. Methods Appl. Mech. Engrg. 158 (1998) 269–300.

[28] T. Laursen, G. Love, Improved implicit integrators for transient impact problems; geometric admissibility within the conserving framework, Int. J. Num. Meth. Engr. 53 (2) (2002) 245–274.

[29] P. L. Tallec, C. Rahier, A. Kaiss, Three-dimensional incompressible viscoelasticity in large strains: Formulation and numerical approximation, Comput. Methods Appl. Mech. Engrg.

[30] R. Abraham, J. Marsden, Foundation of mechanics, Springer-Verlag, 1988.

[31] P. Hauret, Méthodes numériques pour la dynamique des structures non-linéaires incompressibles à deux échelles (Numerical methods for the dynamic analysis of two-scale incompressible nonlinear structures), Ph.D. thesis, Ecole Polytechnique (2004).

[32] P.-G. Ciarlet, Mathematical Elasticity, North Holland, 1988.

[33] O. Gonzalez, Time integration and discrete hamiltonian systems, Journal of Nonlinear Science 6 (1996) 449–467.

[34] T. Hughes, The Finite Element Method, Linear Static and Dynamic Finite Element Analysis, Prentice-Hall, 1987.

[35] T. Laursen, Computational contact and impact mechanics, Springer, 2002.

[36] J. Simo, T. Laursen, Augmented Lagrangian treatment of contact problems involving friction, Comput. Struct. 42 (1992) 97–116.

[37] P. L. Tallec, Handbook of Numerical Analysis, Vol. 3, North Holland, 1994, part 2: Numerical methods for solids.

[38] P. L. Tallec, J. Mouro, Fluid structure interaction with large structural displacements, Comp. Meth. Appl. Mech. Eng. 190 (24-25) (2001) 3039–3068.

[39] J.-F. Gerbeau, T. Lelièvre, C. L. Bris, Simulation of MHD flows with moving interfaces, Journal of Computational Physics 184 (2003) 163–191.

[40] C. Farhat, M. Lesoinne, P. L. Tallec, Load and motion transfer algorithms for fluid/structure interaction problems with non-matching discrete interfaces: Momentum and energy conservation, optimal discretization and application to aeroelasticity, Comp. Meth. Appl. Mech. Eng. 157 (1-2) (1998) 95–114.

[41] P. L. Tallec, P. Hauret, Energy conservation in fluid-structure interactions, in: P. N. Y. Kuznetsov, O. Pironneau (Eds.), Numerical methods for scientific computing, variational problems and applications, CIMNE, Barcelona, 2003.

[42] P. L. Tallec, P. Hauret, J. Gerbeau, M. Vidrascu, Fluid structure interaction problems in large deformations, C. R. Acad. Sci. Paris– submitted.